Compositional variation of apatite from rift-related alkaline igneous rocks of the Gardar Province, South Greenland

Revision 2

Sara Ladenburger[1], Michael A.W. Marks[1,*], Brian Upton[2], Peter Hill[2,+], Thomas Wenzel[1], Gregor Markl[1]

[1] Eberhard Karls Universität Tübingen, Mathematisch-Naturwissenschaftliche Fakultät, FB Geowissenschaften, Wilhelmstrasse 56, D-72074 Tübingen, Germany

[2] School of Geosciences, Grant Institute, University of Edinburgh, West Mains Road, Edinburgh EH9 3JW, UK.

[+]Peter Hill: deceased.

* corresponding author Email: michael.marks@uni-tuebingen.de

Keywords: alkaline rocks, apatite, compositional variation, petrogenetic indicator

Abstract - Textural and compositional variations of apatite from rift-related gabbros, syenogabbros, syenites, quartz-syenites and nepheline syenites of the Mid-Proterozoic Gardar Province (South Greenland) are presented and compared to apatite compositions from other rock suites.

The observed zoning textures of apatite are interpreted to represent (i) primary growth zonation (concentric and oscillatory) that formed during magmatic differentiation and (ii) secondary irregular overgrowths, patchy zonation and resorption textures, assigned to metasomatic overprinting due to interaction with fluids/melts and intra-crystalline diffusion. Compositional variation in the apatites is mainly due to coupled substitutions of Ca and P by variable amounts of Si, Na and REE, which show increasing concentrations during magmatic differentiation. Further, F concentrations in apatites increase from gabbroic through syenogabbroic to syenitic rocks, whereas Cl concentrations show the opposite trend.

Compared to apatite compositions from gabbroic, dioritic, and granitic rocks in general, apatites from alkaline rock suites are characterized by exceptionally high contents of REE and Si and in some alkaline rocks they attain Sr contents comparable to those reported from carbonatites. Typical low Mn and S contents are probably a result of low oxygen fugacity during crystallization at relatively high temperatures.

Introduction

Apatite is a common accessory mineral in a wide range of igneous rocks (Liferovich and Mitchell 2006; Marks et al. 2012; Piccoli and Candela 2002; Sha and Chappell

1999; Seifert et al. 2000; Teiber et al. 2015a). The apatite supergroup covers minerals with the structural formula $M_5(TO_4)_3X$ including phosphates, arsenates, sulfates, vanadates, and silicates that can exhibit a wide range of solid solution (Pasero et al. 2010). In igneous apatites, the major cation in the M site is generally Ca, the T site is mainly occupied by P and the X site by F, OH, and Cl (e.g., Piccoli and Candela 2002; Pan and Fleet 2002). Geochemically important elements including Sr, Na, Fe, Mn, Rare Earth Elements (REE), Si, and S substitute for Ca and P (cf., Belousova et al. 2002; Chu et al. 2009; Pan and Fleet 2002; Piccoli and Candela 2002; Marks et al. 2012; Sha and Chappell 1999; Teiber et al. 2015a; Zirner et al. 2015).

Apatite compositions are controlled by temperature, pressure, oxygen fugacity, and composition of coexisting phases as well as by the bulk composition of the host magma (Ayers and Watson 1993; Belousova et al. 2001; Boyce and Hervig 2008; Chu et al. 2009; Hoskin et al. 2000; Miles et al. 2014; Sha and Chappell 1999; Watson and Green 1981; Parat et al. 2002). Consequently apatite can be a sensitive recorder of magmatic processes (e.g. fractional crystallization or magma mixing) as well as of subsequent hydrothermal overprinting, metasomatism, and re-equilibration during cooling (e.g., Harlov and Föster 2003; Harlov et al. 2005; 2011; Chu et al. 2009; Rønsbo 2008; Tepper and Kuehner 1999; Wang et al. 2014; Teiber et al. 2015b). In igneous rocks, apatite may occur as an early crystallizing phase, precipitating over a very long crystallization interval or may start crystallizing very late (e.g., Boudreau et al. 1993; Hoskin et al. 2000).

On the basis of an extensive data set on apatite compositions from variably differentiated rift-related alkaline igneous rocks, we aim to (1) evaluate the potential of apatite for monitoring magmatic and hydrothermal processes in such rock types

and (2) compare these data with apatite compositions from gabbroic, dioritc and granitic rocks from non-alkaline associations and from carbonatites (e.g. Belousova et al. 2001; Piccoli and Candela 2002; Sha and Chappell 1999; Teiber et al. 2015a).

Geological background

The Gardar Province in South Greenland represents an uplifted and eroded continental rift province of Mesoproterozoic age (see Upton et al. 2003 for a recent review). Between 1350 and 1140 Ma, a thick (~3500 m) sequence of lavas and sediments (the Eriksfjord Formation) accumulated (Poulsen 1964; Larsen 1977; Halama et al. 2003), which was intruded by a large number of dike rocks and several composite plutonic complexes (**Fig. 1**). The mostly Paleoproterozoic (Ketilidian) country rocks consist of calc-alkaline granitoids of the Julianehåb batholith that formed between 1850 and 1725 Ma after presumed subduction of an oceanic plate beneath the Archean craton to the north (Garde et al. 2002). In the NW of the province, Archean high-grade gneisses form the country rocks for some of the Gardar intrusives (Allaart 1976).

The dikes vary in composition from mafic to salic (basaltic to trachytic, phonolitic, and rhyolitic) and also include lamprophyres and carbonatites. These strike mostly WNW-ESE and NE-SW following zones of inferred lithospheric thinning and graben development (Upton et al. 2003; Upton 2013). Two major dike swarms are located in the Tugtutôq-Ilímaussaq and the Nunarssuit-Isortoq zones. Abundant anorthosite xenoliths in some of the dike rocks imply the presence of a large anorthosite body underlying South Greenland (Bridgwater 1967; Bridgwater and Harry 1968).

The intrusive complexes consist of syenites, nepheline syenites, alkali granites, gabbros, syenogabbros, and carbonatites (in order of decreasing abundance). With few exceptions, they follow either a SiO_2-undersaturated or a SiO_2-oversaturated trend, depending mainly on crustal contamination (e.g. Marks et al. 2003; 2004a; Stevenson et al. 1997). The rocks crystallized about 3-5 km below the surface and it is likely that most of the complexes had surface expressions (Upton 2013). Most of the larger Gardar intrusions are characterized by layered cumulates. The remarkable abundance of cumulate layering (attributed to crystal sinking or floating), together with unusually coarse-grained textures and extensive in situ differentiation, has been related to low viscosities in F-rich melts (Upton et al. 2003). Previous field and experimental investigations indicate that these relatively reduced melts evolved through Fe-enrichment to extremely alkaline differentiates (e.g. Upton 2013; Giehl et al. 2012). Some of them that contain eudialyte-group minerals ($Na_{15}Ca_6Fe_3Zr_3Si(Si_{25}O_{73})(O,OH,H_2O)_3(Cl,OH)_2$) and other Na-Zr-Ti silicates are classified as agpaitic rocks. They represent some of the most evolved magmatic rocks on Earth (e.g., Bailey et al. 2001; Sørensen 1997; Marks et al. 2011). Based on the available age data, the intrusive rocks are divided into older and younger Gardar intrusions (Upton 2013). Older Gardar intrusions include Grønnedal-Ika, Kûngnât, Motzfeld, North Qôroq, and North Motzfeld with intrusive ages between about 1300 and 1250 Ma. Most other intrusives (e.g., Isortoq, Tugtutôq, Puklen, Ilímaussaq) belong to the Younger Gardar period with ages between about 1180 and 1140 Ma and are interpreted as constituting a coherent magmatic system (Upton 2013).

Material and Methods

For this study we used otherwise well-characterized sample material from the Grønnedal-Ika complex (Emeleus 1964; Blaxland et al. 1978; Halama et al. 2005); the Kûngnât complex (Upton et al. 2013); the Motzfeldt complex (Jones 1980; Jones and Larsen 1985; Schönenberger and Markl 2008; McCreath et al. 2012); the Isortoq dike swarm (Bridgwater and Harry 1968; Bridgwater and Coe 1970; Upton and Emeleus 1987; Halama et al. 2002; 2004); the Tugtutôq region, where two major giant dike complexes (Older and Younger Giant Dike Complexes; OGDC and YGDC) are distinguished (Upton and Thomas 1980; Upton et al. 1985 Upton 2013); the nearby island of Igdlutalik (Upton et al. 1976; Upton 2013); the Puklen complex (Pulvertaft 1961; Parsons 1972; Finch et al. 2001; Marks et al. 2003); and the Ilímaussaq complex (Ferguson 1964; Larsen and Sørensen 1987; Bailey et al. 2001; Marks et al. 2004a; Krumrei et al. 2006; Marks and Markl in press). The intrusion is the type locality of agpaitic rocks, as well as for a lot of uncommon (and some unique) minerals including a number of Nb-, Zr-, REE-rich minerals. An ENE-WSW trending peralkaline (agpaitic) phonolite dike is spatially associated with the Ilímaussaq complex. This 10-30 m wide dike is traceable for about 18 km and provides insight into the nature of the magma(s) from which the Ilímaussaq agpaities formed (e.g., Larsen & Steenfelt 1974; Marks and Markl 2003).

The textures and compositions of apatite from these localities are described below. This includes previously published apatite data from Ilímaussaq (Rønsbo 1989; 2008; Zirner et al. 2015) and the North Qôroq complex (Rae et al. 1996), for comparison. Accordingly, we present apatite compositions from a continuous spectrum of broadly co-genetic, rift-related igneous rocks ranging from gabbros, syenogabbros, syenites, quartz- and nepheline syenites to highly evolved agpaites (**Table 1; Fig. 2**).

Sample Material

From the Grønnedal-Ika complex, five samples of the coarse-grained and layered nepheline syenites were studied. Major magmatic mineral phases are cumulus clinopyroxene, nepheline, alkali feldspar, and Fe-Ti oxides with minor amounts of apatite. Amphibole is an intercumulus phase in sample GM 1531 and biotite is present only in sample GM 1559.

From the Kûngnât complex, two samples of coarse-grained gabbros, one of syenogabbro, and seven of syenite were investigated. The gabbros consist of olivine, Fe-Ti oxides, plagioclase, apatite, and sulfides. Clinopyroxene and alkali feldspar are late-crystallizing phases, and biotite is present as reaction fringes around the oxides. The modal amount of alkali feldspar increases at the expense of plagioclase in the syenogabbros; Fe-Ti oxide and apatite reach their modal peaks in these rocks. In the syenites the feldspars are all perthitic alkali feldspars, accompanied by olivine, clinopyroxene, Fe-Ti oxides, and apatite. Intercumulus amphibole is ubiquitous and, as in the mafic rocks, reaction fringes of biotite surround the oxides. In the more highly differentiated syenites interstitial quartz is present.

From the Motzfeldt complex, three samples of coarse-grained nepheline syenite were studied. They mainly consist of amphibole, clinopyroxene, tabular alkali feldspar, nepheline, and Fe-Ti oxides with accessory zircon, apatite and calcite. Further, a larvikite sample contains olivine, clinopyroxene, amphibole, nepheline, alkali feldspar, plagioclase, apatite, and Fe-Ti oxides. The Fe-Ti oxides are also typically rimmed by biotite.

From the Isortoq dike swarm, nine samples were selected. One was an anorthosite xenolith mainly containing plagioclase, clinopyroxene, and Fe-Ti oxides, with minor amphibole, quartz, and apatite. A larvikite sample consists of clinopyroxene, Fe-Ti

oxides, plagioclase, and alkali feldspar, with subordinate interstitial quartz, amphibole, and biotite and accessory apatite and zircon. A sample of olivine gabbro contains subhedral olivine, plagioclase, and interstitial clinopyroxene as major components and minor apatite and Fe-Ti oxides. Olivine and Fe-Ti oxides are commonly rimmed by biotite. A further six samples were selected from the Isortoq Giant Dikes. The gabbroic samples from Giant Dikes 1 and 3 are coarse-grained and contain plagioclase, alkali feldspar, olivine, interstitial clinopyroxene, Fe-Ti oxides, and apatite. The syenitic samples lack plagioclase and olivine but contain euhedral to subhedral clinopyroxene, together with amphibole and epidote. Transition from gabbro to syenite is exemplified by the syenogabbro sample. In all Giant Dike samples, olivines, clinopyroxenes, and/or Fe-Ti oxides have biotite overgrowths.

From the Tugtutôq region we investigated six gabbros, four syenograbbros, six syenites, one pulaskite, and three foyaites from the OGDC and YGDC. The gabbroic samples contain plagioclase, olivine, clinopyroxene, Fe-Ti oxides (some rimmed by biotite) and apatite. Syenitic samples (including pulaskite and foyaites) lack plagioclase and olivine but contain additional amphibole. Syenitic rocks of the OGDC are invariably nepheline-bearing, whereas some syenites from the YGDC contain minor amounts of quartz. As at Isortoq, syenogabbros from the Tugtutôq region display the transition from gabbro to syenite with minor amounts of plagioclase still present in the latter.

The pantelleritic, trachyte dike from Igdlutalik is remarkable for containing narsarsukite ($Na_2(Ti,Fe^{3+})Si_4(O,F)_{11}$) phenocrysts. They lie in a fine-grained devitrified matrix showing flow-banding (defined by differing conentrations of finely dispersed albite, aegirine, biotite and Fe-Ti oxides). Minor components are apatite,

pectolite, zircon, nordite ($Na_3SrCeZnSi_6O_{17}$), emeleusite ($Li_2Na_4Fe_2^{3+}Si_{12}O_{30}$), unidentified REE silicate(s), and calcite.

From the Puklen complex, six syenite and two peralkaline granite samples were investigated. The syenites are medium- to coarse-grained and contain alkali feldspar, clinopyroxene, amphibole, Fe-Ti oxides, apatite, and zircon as primary magmatic phases, with aenigmatite ($Na_4[Fe^{2+}_{10}Ti_2]O_4[Si_{12}O_{36}]$) and quartz occuring as a late magmatic phases in two samples. The peralkaline granites consist of alkali feldspar, quartz, clinopyroxene, amphibole, zircon, and scarce apatite.

Methods

The major- and minor-element compositions of the apatites from Grønnedal-Ika, Motzfeldt, Isortoq and Puklen were determined using a JEOL 8900 electron microprobe (EMPA) operating in wavelength-dispersive (WDS) mode at the Fachbereich Geowissenschaften, Tübingen University, Germany. A beam current of 10 nA, an acceleration voltage of 15 kV and a defocused beam diameter of 10 µm were applied to achieve constant count rates during peak counting times and to avoid migration of Na, Ca, P, F, and Cl. To further minimize this potential problem, we avoided analyses where the electron beam was parallel to the apaites c-axis as much as possible (Goldoff et al. 2012; Stormer et al. 1993; Wang et al. 2014). Details on standard materials used for calibration and analytical conditions are given in Teiber et al. (2015a). The well-characterized Durango apatite was periodically re-analyzed to ensure consistency between the analytical sessions. Data reduction was performed using the internal ZAF correction of JEOL (Armstrong, 1991). Apatites from Kûngnât, Tugtutôq and Igdlutalik were analyzed by Peter Hill at the Institut für Petrologie, Universität Wien using a Cameca SX100 applying a beam current of 20

nA, an acceleration voltage of 20 kV and a focused beam. Therefore, concentrations of halogens should be interpreted with caution, as the mobiliy of F and less so Cl during analyses was not considered at the time of their analysis.

Results

Apatite is much more abundant in the gabbroic samples than in the syenites and is rare in the peralkaline granites. It is regarded as an early magmatic phase in all investigated samples as it occurs as inclusions in all the other rock-forming minerals and along grain boundaries. Apatite typically occurs as euhedral to subhedral prisms with diameters <100 µm and lengths of <800 µm, with no large differences between the various localitites and rock types. In peralkaline granites from the Puklen complex, apatite crystals are too small (generally <10 µm in diameter) for analysis. In a few samples, additional acicular apatites with diameters <15 µm and lengths of up to about 800 µm occur. Such apatites could not be reliably analyzed by EMPA.

Apatite zoning textures

Based on BSE imaging, apatites from Isortoq, Tugtutôq, and Igdlutalik are homogeneous. In contrast, apatites from composite intrusive complexes display various types of zoning, which we summarize in the following. Zonal textures of apatites from the Ilímaussaq and North Qôroq are described in detail in Rønsbo (1989; 2008), Zirner et al. (2015), and Rae et al. (1996).

Apatites from Grønnedal-Ika display variable zoning textures. Some crystals appear homogeneous in BSE images, some show concentric and oscillatory zoning, whilst others display zoning with dark cores (sometimes euhedral, sometimes rounded) and

brighter rims (**Figs. 3a-c**). Furthermore, many apatite grains are overgrown by irregularly formed, discontinuous, and mostly <5 µm wide very bright rims (termed overgrowth textures in the following), which have compositions with higher average atomic numbers (**Figs. 3a, c and d**).

In the Motzfeldt syenites most apatites are concentrically and oscillatory zoned. As in the Grønnedal-Ika samples, a small proportion of the apatites display zoning with euhedral to rounded cores and BSE imaging reveals abrupt to gradational compositional changes across these minerals (**Figs. 4a-c**). The common overgrowth textures, as observed in the Grønnedal-Ika, are, however, mostly absent. In one sample (JS 104) patchy zoning is observed (**Fig. 4d**). Apatites from the larvikite (JS 215) appear homogeneous in BSE images.

Apatites from Puklen are mostly homogeneous (**Fig. 4e**). However, in sample GM 1615, otherwise homogeneous apatites are overgrown by irregular and discontinuous bright rims (**Fig. 4f**), similar to textures found the Grønnedal-Ika rocks.

Compositional variability

The compositional variability of the Gardar apatites is illustrated in **Figs. 5-7**, where the samples of each locality are shown from left to right by decreasing X_{Mg} of their respective whole-rock and mafic mineral compositions. Apatite formulas were normalized to eight cations, assuming stoichiometry. The amount of OH was calculated assuming charge balance on a fully occupied OH-site (sum of F + Cl + OH = 1 apfu) and the potential incorporation of CO_3 was not considered further here. The full dataset is available as an **electronic supplement** attached to this paper.

During EMPA, La and Ce were analyzed as proxies for the total REE content of the apatites. Most of the these apatites contain <4 wt.% La_2O_3 + Ce_2O_3 **(electronic**

supplement). In such analyses, the heavier LREE (Pr, Nd, Sm), the MREE and the HREE would be close to or below the detection limit of EMPA, which would render most of these values meaningless. Therefore, we did not include heavier LREE, MREE and HREE in our EMPA protocol. Some apatites of the evolved rocks from Ilimaussaq are very REE-rich (Rønsbo 1989; 2008; Zirner et al. 2015), and the EMPA totals for such apatites imply up to about 5 wt.% missing REE. However, because of the LREE-rich and HREE-poor nature of such apatites (Zirner et al. 2015), and because of the high masses of REE in general, the effects on the formula calculation are relatively minor. A comparison between EMPA and LA-ICP-MS data (Zirner et al. 2015) for such apatites show that the omission of heavier REE´s during EMPA has no significant effect on the derived conclusions.

Substitutions on the Ca-site - Apatites from the relatively primitive gabbroic rocks have low La + Ce contents (mostly <0.05 apfu), whilst those from miaskitic syenites are generally higher in La + Ce (mostly 0.05 - 0.15 apfu). Exceptionally high LREE contents occur in agpaitic syenites (up to 0.75 apfu) and in overgrowth textures from the miaskitic syenites (up to 0.56 apfu) of the Ilímaussaq complex (**Fig. 5a**; Rønsbo 1989; 2008; Zirner et al. 2015). The within-sample variation of La + Ce contents is much larger in the syenitic rocks than in the gabbroic rocks. In samples from a given locality, the LREE contents generally increase with degree of differentiation, although this trend is less clear for the Gronnedal-Ika and Motzfeld samples. Invariably the LREE contents increase from core to rim (**Fig. 6**).

As in the case of La + Ce, Na contents of the apatite increase from gabbroic (<0.03 apfu) to syenitic rocks (mostly between 0.02 and 0.1 apfu). Exceptionally high Na contents occur in apatites from evolved syenites (foyaites) from Tugtutôq (up to 0.42

apfu) and in agpaites from Ilímaussaq (up to 0.56 apfu), but not in the overgrowth textures from the Ilímaussaq miaskitic syenites as was observed for LREE (**Figs. 5a and b**). In samples from a given locality, Na contents generally increase with degree of magma differentiation, although this is less clear in some syenitic complexes. The Na concentrations are higher in the cores than at the rims of concentrically zoned crystals. In those with rounded cores, however, Na contents show no systematic variation (**Fig. 6**).

Contents of Sr vary from 0.001 – 0.10 apfu Sr, and are highest in apatites from the Ilímaussaq agpaites (**Fig. 5c**). Relatively high and variable Sr contents (up to 0.06 apfu) also occur in apatites from the Grønnedal-Ika and the Motzfeldt miaskitic syenites. Apatites from all other intrusive complexes (North Qôroq, Kûngnât and Ilímaussaq, exluding the agpaitic rocks) and rocks from the Isortoq and Tugtutôq regions are relatively poor in Sr (<0.02 apfu). In contrast to REE contents (see above), the Sr contents of apatites from a given locality show no obvious changes with degree of differentiation. Yet, Sr contents in concentrically zoned apatites are higher in the cores than at the rims of crystals, very similar to Na. In grains with rounded core textures, however, this is not always the case (**Fig. 6**).

The FeO and MnO contents for all investigated apatites are low (<0.9 and <0.1 wt%, respectively), and show no systematic differences between localitites, rock types, or degree of differentiation (**Figs. 5d and e**).

Substitutions on the P-site - The Si contents of apatite are generally <0.04 apfu in the gabbros and syenogabbros, reaching about 0.27 apfu Si in the miaskitic syenites and attaining the highest levels in secondary overgrowth textures and agpaites from Ilímaussaq (up to 1.01 apfu; **Fig. 5f)**. Zoning profiles and core-rim variations of

apatites show increasing concentrations of SiO_2 from core to rim, which behave in a very similar manner as the REE contents (**Fig. 6**). Like the REE (and to some extent Na), Si increases with degree of differentiation in any single intrusive complex. There is, however, large data scatter within and between samples, especially in the syenites.

Sulfur and As contents in apatite are mostly below the EMPA detection limit (around 230 µg/g for SO_3 and 290 µg/g for As_2O_5). Only in a few analyses do the S contents rise to 0.07 wt% SO_3 (0.004 apfu S), with As reaching 0.06 wt% As_2O_5 (0.003 apfu As).

Substitutions on the OH-site - Apatites from most of the investigated samples are fluorapatite, as is typical for most igneous rocks (Piccoli and Candela 2002). A few analyses from the more mafic samples from Tugtutôq and Kûngnât yield low sums of (F + Cl), apparently indicating the presence of a significant hydroxylapatite component (**Fig. 7**). Note that F (and less so Cl contents) for these analyses should be interpreted with caution, as the mobility of F and less so Cl during analyses was not considered at the time of their analysis. However, F and Cl contents for the Isortoq samples are partly equally low although these samples were analyzed with appropriate conditions for halogens (see methods section for details). The potential incorporation of carbonate is not discussed here, as no data for C for these apatites are available.

In general, F contents are lowest in apatites from the gabbroic rocks and reach much higher values in the syenites (**Fig. 7a**). In apatites from the Isortoq region a clear F increase in the apatite with differentiation is indicated. Fluorine contents are known to increase from primitive towards more evolved rocks (Belousova et al. 2002; Sha and

Chappell 1999; Teiber et al. 2015a). Such a trend is, however, not observed in the sample sets from the investigated syenitic complexes, where there is relatively little change in apatite compositions. Furthermore, there are no major differences in apatite compositions from the different syenitic complexes although apatites from the Motzfeld complex are slightly poorer in F than those from the Grønnedal-Ika, Puklen, and Ilímaussaq complexes.

Chlorine contents (up to 0.49 wt%; 0.05 apfu Cl) show a crude inverse correlation with F and are relatively high in the gabbroic rocks but very low in syenites from the various intrusive complexes (**Fig. 7b**). The apatites from the two larvikites have notably higher Cl contents than those from the other samples from the same localities, irrespective of whether it is the most primitive (Motzfeld complex) or the most evolved (Isortoq) rock.

Predominant substitution mechanisms - The contents of Sr, Fe, Mn, S, and As in apatites from the Gardar Province are generally low and their variations do not show any obvious systematic behavior in terms of rock type and degree of differentiation. Apart from some variation in F and Cl, most of the compositional variation in the apatites is related to their Na, Si, and REE contents. Positive correlations between REE, Si, and Na (**Fig. 8**) are consistent with the incorporation of REE by a combination of the following charge-compensating substitution mechanisms:

$$Ca^{2+} + P^{5+} \leftrightarrow REE^{3+} + Si^{4+} \quad (1)$$

$$2\,Ca^{2+} \leftrightarrow REE^{3+} + Na^{+} \quad (2)$$

Both substitution mechanisms have been described before (e.g., Pan and Fleet 2002; Fleet et al. 2000; Zirner et al. 2015; Rønsbo 1989, 2008). Their combined appearance may be related to the alkalinity and/or silica activity of the magma from

364 which these apatites crystallize, if these substitutions are not limited by the overall
365 abundance of REE's in the magma (see below).

366

367 # Discussion

368 **Interpretation of apatite zoning textures**

369 The compositional variability of apatites records magmatic processes (e.g. fractional
370 crystallization, magma mixing, magmatic degassing). The textural and chemical
371 signatures may be overprinted by post-magmatic processes, such as hydrothermal
372 replacement and diffusive reequilibration (Boyce and Hervig 2008; Dempster et al.
373 2003; Hinton and Paterson 1994; Jolliff et al. 1989; Rae et al. 1996; Shore and
374 Fowler 1996; Streck 2008; Tepper and Kuehner 1999; Harlov and Förster 2003). The
375 zoning textures described above can be used to elucidate the evolution of the
376 magma from which the apatite crystallized during differentiation and post-magmatic
377 processes (e.g. hydrothermal modification).

378 Homogeneous (i.e. unzoned) apatites occur mainly in the more primitive Isortoq and
379 Tugtutôq samples and also in the larvikite from Motzfeld. The other rock-forming
380 minerals in these rocks also have little or no zoning (e.g., Halama et al. 2004). For
381 these rocks fast crystallization under dry conditions was inferred, obviously
382 minimizing compositional zoning during growth (e.g., Upton and Thomas, 1980;
383 Halama et al. 2004). Furthermore some of these rocks contain acicular apatite, which
384 grew rapidly due to strong undercooling or loss of volatiles (Reid et al. 1983; Sha
385 1995; Wyllie et al. 1962; Zirner et al. 2015).

386 Concentrically zoned apatites, seen mainly in Motzfeldt and Grønnedal-Ika, are due
387 to compositional changes in the magma during growth, which is attributed e.g. to

magma mixing and differentiation processes (e.g. Streck 2008). The core-rim traverses in such apatites show increasing Na, Si, and REE and decreasing Sr (**Fig. 6**). Similar trends are also recorded for the evolution from gabbros to syenites in the Isortoq and Tugtutôq samples (**Fig. 5**). These trends may partly reflect magma evolution during fractional crystallization but are also partly controlled by the coupled substitution governing the compositional variability of apatite (Tepper and Kuehner 1999), which will be discussed in more detail below. However, fine-scale oscillatory zoning is generally interpreted as reflecting non-equilibrium magmatic processes (e.g., Shore and Fowler 1996). The composition of the very thin (<5 μm) growth layers depends on the relative element diffusion rates for the elements in the melt and crystal (Dempster et al. 2003; Shore and Fowler 1996; Tepper and Kuehner 1999). Such zoning is only rarely observed in apatites from Grønnedal-Ika and Motzfeldt (**Figs. 3 and 4**). These apatites probably crystallized in segregated melt pockets over longer crystallization intervals.

Apatites with rounded cores have been attributed to inheritance from country rocks, magma mixing, changes in crystal/melt element partitioning, or kinetic effects (Tepper and Kuehner 1999; Sha and Chappel 1999; Wang et al. 2014). Core-to-rim traverses show increases in Si and REE but no systematic changes in Na and Sr (**Fig. 6**). These textures may result from incomplete, sub-solidus, intra-crystalline diffusion as different crystals show different stages from euhedral to completely rounded cores (**Figs. 3 and 4**). The zoning of certain elements in apatite with rounded cores may have been controlled by their respective substitution mechanism (Tepper and Kuehner 1999). For example Sr, which substitutes for Ca, does not show strict core-to-rim variations (**Fig. 6**), whereas REE and Si, which participate in coupled substitutions for Ca, display large core-to-rim variations similar to those of the concentrically zoned apatites (**Fig. 6**). However, Na, which is also involved in

coupled substitutions, shows no distinct trends (**Fig. 6**), and this could be due to differences in diffusion rates, with Sr diffusing faster than Na and Si (Tepper and Kuehner 1999).

Irregular and discontinuous overgrowth textures occur in rocks from Grønnedal-Ika and Puklen (**Figs. 3a, c, d and 4f**) and are very similar to features in the Ilímaussaq apatites that are exceptionally rich in Na, Si, and REE (Rønsbo 1989; 2008; Zirner et al. 2015). Because of their irregular shape, they were ascribed to metasomatic overprint caused by the interation with evolved melts/fluids. Similar patchy zonation in samples from Motzfeldt (**Fig. 4d**), North Qôroq (Rae et al. 1966) and Ilímaussaq (Zirner et al. 2015) is attributed to the effects of the metasomatizing fluids.

Significance of Sr contents in apatites from the Gardar Province

In general, the concentration of Sr in apatites decreases with magmatic differentiation because of the preferred partitioning of Sr into plagioclase (e.g.; Belousova et al. 2001; 2002; Chu et al. 2009). There is, however, no correlation between Sr contents and the degree of differentiation in the investigated samples from the Gardar province. The data indicate that apatites from the more primitive rocks do not contain more Sr than those from the evolved rocks - neither when samples of a single suite nor those from different localitites are compared (**Fig. 5**). This is probably related to the early magmatic evolution of most of the evolved Gardar rocks. These are assumed to have experienced extensive plagioclase fractionation (e.g., Bridgwater 1967; Bridgwater and Harry 1968; Halama et al. 2002), which could have caused the generally low Sr contents in apatite.

Apatites from Grønnedal-Ika are richer in Sr than those from the other Gardar rocks (except the Ilímaussaq agpaites) and their Sr contents decrease from core to rim

(**Figs. 5 and 6**). Similarily, Sr contents of clinopyroxene and amphibole from Grønnedal-Ika are significantly higher than in other Gardar syenites and in contrast to minerals and rocks from other Gardar complexes, lack any Eu anomalies (Marks et al. 2004b). Furthermore, Grønnedal-Ika hosts the only large carbonatite body that intrudes Archean basement rocks. Isotopic data for this complex indicate a slightly different magma source and the absence of any significant crustal contamination (Halama et al. 2005). Therefore, the early magmatic history of the Grønnedal-Ika complex may have been slightly different from that of the other Gardar rocks, potentially lacking extensive fractionation of plagioclase. This implies that the magma source of the Grønnedal-Ika intrusions was richer in Sr than in the case of the other Gardar complexes, which would be a primary feature, not necessarily related to the associated carbonatite.

Anomalously, a late-stage agpaitic vein from Ilímaussaq has apatite with even higher Sr contents, although the apatites in the less-evolved rocks of the complex contain very Sr-poor apatites (**Fig. 5**; Zirner et al. 2015). This shows that the general assumption of decreasing Sr contents in apatite with increasing differentiation is not applicable to such rock types. Because of their evolved character, minerals and rocks from Ilímaussaq are exceptionally Sr-poor (Bailey et al. 2001; Marks et al. 2004b; Schilling et al. 2011). Further, it is known that Sr is slightly compatible with alkali feldspar (which is the dominant fractionation phase) in peralkaline systems (e.g., Henderson and Pierozynski 2012), which makes the occurrence of relatively Sr-rich apatite during the latest magmatic stages of the complex even more remarkable. Although the reason for the late Sr-rich apatites in Ilímaussaq is obscure, it may be related to the mobilization of Sr during late-magmatic to hydrothermal stages, rather than Sr enrichment during evolution through fractional crystallization.

The combined incorporation of REE, Na and Si in apatite

The concentrations of REE in apatite increase during the evolution from relatively primitive to more-evolved rocks at all of the investigated localitites. This is accompanied by a Si increase and partly (but not always) by an increase in Na (**Figs. 5 and 6**). This agrees with previous investigations on apatite from a wide range of magmatic rocks (e.g. Belousova et al. 2002; Chu et al. 2009; Nash 1984; Seifert et al. 2000; Sha and Chappell 1999). As REE are strongly compatible in apatite (e.g., Hoskin et al. 2000; Watson and Green 1981; Prowatke and Klemme 2006), apatite is more sensitive to changes in REE concentrations in magmas than most rock-forming silicate minerals (Cherniak 2000).

Through the coupled substitution of REE with Si and REE with Na for Ca and P (see above), any secondary or post-magmatic change in the REE concentrations would require a complementary redistribution of Si and Na. Tepper and Kuehner (1999) observed that REE diffusion rates in apatite are an order of magnitude slower if the coupled substitution mechanism is $Ca^{2+} + P^{5+} \leftrightarrow REE^{3+} + Si^{4+}$, compared to the incorporation of REE^{3+} via the coupled substitution $2Ca^{2+} \leftrightarrow REE^{3+} + Na^{+}$. However, Cherniak (2002) has suggested that there is no difference in REE mobility within apatites with regard to the particular coupled substitution mechanism by which the REE are charge balanced.

Zoning patterns observed for apatites in this study support the arguments of Tepper and Kuehner (1999) that the compositional zoning for REE and Si is always preserved, but partly erased for Na, especially in those apatites with rounded core textures (**Fig. 6**). This underlines the high potential for REE and Si contents in apatite to be used as a powerful petrogenetic indicator, but less so for Na. In our study,

increasing Na concentrations related to differentiation processes are only observed at localitites that include relatively primitive and evolved rocks (e.g., Isortoq), whereas in evolved syenitic complexes (e.g., Puklen and Motzfeld) this relationship is much less clear (**Fig. 5**). We assign this to the post-magmatic hydrothermal overprinting typical for plutonic alkaline complexes. We further suggest that this is preserved in apatites from syenitic complexes, as these show a relatively wide range for the fast-diffusing elements (e.g. Na and Sr) within single samples (**Fig. 5**; see above). This is most pronounced in samples from the Grønnedal-Ika and Motzfeldt complexes. Apatites from these complexes show abundant zoning textures that are probably related to the interaction with evolved fluids/melts, such as rounded core textures, patchy zoning and irregular overgrowths (**Figs. 3 and 4**; Rae et al. 1996; Zirner et al. 2015). Accordingly, primary magmatic processes may be distinguished from metasomatic processes on the basis of textural arguments. From these observations and the fast diffusion rates of Na and Sr (Cherniak 2000; Cherniak and Ryerson 1993; Tepper and Kuehner 1999), the overall reliability of these two elements as petrogenetic indicators for magmatic processes is poor, at least for alkaline plutonic rocks.

There is no direct link between the relative importance of REE coupled substitution mechanisms involving Si and the Si contents of the host melts: Apatites from quartz-bearing syenites of Puklen are not dominated by this coupled substitution meachanism unlike the apatites from the syenites of the Ilímaussaq complex (**Fig. 8**). Only in apatites from the agpaitic rocks does the REE coupled substitution mechanism involving Na become dominant (although not in all cases; Zirner et al. 2015; **Fig. 8**). Apatites from the other nepheline syenites fall in between these two extremes as do apatites from both Si-poor (carbonatites) and Si-rich magmas (granitic rocks; Sha and Chappell 1999; Teiber et al. 2015a). The amount of Si in

apatite is a good petrogenetic indicator, within a given rock association, for reconstructing, (for example) magma differentiation paths. However, the Si contents in apatite do not provide direct information about the melt compositions e.g., SiO_2 over- or undersaturation. This suggests, that the amount of Si substitution in apatite is influenced by the avalailability of REE involved in the frequently observed coupled substitition $Ca^{2+} + P^{5+} \leftrightarrow REE^{3+} + Si^{4+}$ (Pan and Fleet 2002; Fleet et al. 2000; Zirner et al. 2015; Rønsbo 1989; 2008).

Comparison between apatite from alkaline rocks and other rock types

In the following discussion the compositional variation of apatites from the Gardar Province is compared to that from investigations of (1) alkaline rock suites of the Pilansberg complex (South Africa; Liverovich and Mitchell 2006) and the Tamazeght complex (Morocco; Wang et al., unpublished data); (2) carbonatites and phoscorites from Russia, Canada, USA, Brazil, Australia, Namibia, Tanzania, Kenya, Finland, Norway and Germany; (3) gabbroic rocks from Canada, USA, China, Australia, South Africa and Zimbabwe; (4) dioritic rocks from Canada, China, Germany, and the Tibetan plateau; (5) biotite (± amphibole) granitoids (including monzonites, granodiorites, and granites) from Australia, Scotland, Greece, Germany, and the Tibetan plateau; and (6) muscovite-bearing granites from Australia, Greece, Germany, and the Tibetan plateau as compiled by Teiber et al. (2015a). In doing so, we try to identify characteristic compositional features of apatite from alkaline rocks as compared to other rock types (**Fig. 9**).

Ca-Sr-Ce systematics - High Sr contents in apatite, approaching end-member composition, are known from carbonatites (**Fig. 9b**) and from kimberlites, orangeites,

and lamprophyres (cf. recent compilation of Chakhmouradian et al. 2002). However, in some apatites from carbonatites, Sr contents are as low as in gabbroic, dioritic and granitic rocks. Sr-rich apatites in such rocks are not restricted to late-stage pegmatites or hydrothermal rocks, but can occur as early magmatic phases. Although the partition coefficient for Sr between apatite and carbonatitic melts is low (<1) compared to that between apatite and silicate melts (typically >1; Prowatke and Klemme 2006; Hammouda et al. 2010), it is suggested that the generally Sr-rich character of carbonatitic melts overhelms this potential effect in many cases (e.g., Teiber et al. 2015a). Likewise, apatite from the Tamazeght and Pilansberg complexes and other alkaline rocks are highly variable but achieve similarly high amounts of Sr (**Fig. 9a;** Chakhmouradian et al. 2002). The extremely evolved agpaitic rocks from Ilímaussaq, however, do not contain unusually Sr-rich apatites. We suggest that this may be caused by differences in the composition of the melts from which these apatites crystallized and differences in the fractionating phase assemblage during magmatic evolution. It is, for example, well established that the early magmatic history of some Gardar complexes is strongly influenced by the early fractionation of large amounts of plagioclase (e.g. Bridgwater 1967; Halama et al. 2002; Upton et al. 2003; Marks et al. 2011). This is in strong contrast to the evolution of the Tamazeght complex (e.g., Marks et al. 2008). As Sr is strongly compatible in plagioclase, Sr-rich apatite in alkaline rocks may only form if no extensive plagioclase fractionation happened during early magmatic stages. This may place direct constraints on parental melt compositions for alkaline rock suites, which are assumed to be alkali basaltic and nephelinitic (e.g., Upton et al. 2003; Kramm and Kogarko 1994; Arzamatsev et al. 2001). We suggest, that Sr-rich apatite occurs only in rocks derived from the latter. The stability of plagioclase in other plutonic rocks (gabbros,

565 diorites, and other granitoids) may be the reason that Sr contents in apatites from
566 these rocks normally do not reach elevated Sr contents (**Figs. 9c and d**).

567 The Ce content (as a proxy for REE in general) is generally low in gabbroic, dioritic,
568 and granitoid rocks but reaches higher values in carbonatites. The most REE-rich
569 apatite-group minerals are known from the Ilímaussaq agpaites (**Fig. 5,** Rønsbo
570 1989, 2008; Zirner et al. 2015). By no means do all the apatites from the other
571 Gardar syenitic rocks, Tamazeght, and Pilansberg reach high Ce contents (**Fig. 9a**).
572 The highest Ce-enrichments found in late-stage overgrowth textures of apatites.
573 These are probably due to interaction with REE-rich residual melts and metasomatic
574 fluids (Zirner et al. 2015). This is most likely related to the exceptional REE-rich
575 nature of the Ilímaussaq melts (e.g., Larsen and Sørensen 1987), obviously not
576 present in alkaline rocks in general and certainly not in gabbroic, dioritic, and
577 granitoid rocks. It was suggested that the Late Gardar mantle source underwent
578 metasomatic enrichment in LREE, Nb, F, and P that was inherited by the basaltic
579 magmas derived from it. Extreme differentiation under reduced conditions ultimately
580 led to the production of the Ilímaussaq agpaites (Upton 2013). In these rocks, large
581 amounts of other REE-rich phases (e.g., eudialyte-group minerals, rinkite, and
582 others; Larsen and Sørensen 1987; Petersen 2001) occur, mainly after apatite
583 crystallization, implying that the residual melts were indeed REE-rich. Extensive
584 apatite crystallization happened during the augite syenite stage prior to agpaite
585 formation where only small amounts of apatite crystallized. During late-magmatic and
586 hydrothermal stages, however, large amounts of various phosphates (e.g., monazite,
587 natrophosphate, vitusite) and silico-phosphates (e.g., steenstrupine, lomonosovite)
588 appear in the Ilímaussaq rocks, especially in so-called hyper-agpaites (e.g. Sørensen
589 and Larsen 2001). Some of these minerals (e.g. steenstrupine) are very REE-rich
590 giving rise to one of the largest REE deposits of the world (Marks and Markl 2015).

591

592 **P-Si-S systematics –** The lowest S contents occur in apatites from muscovite-
593 bearing granites and from alkaline rocks of the Gardar Province and the Pilansberg
594 intrusion. Apatites from carbonatites, gabbros, diorites, and biotite (± amphibole)
595 granitoids are intermediate in S contents. High S contents are found in apatites from
596 the alkaline Tamazeght complex (**Fig. 9**). This probably relates to the redox
597 conditions of the melts from which the apatite crystallized, as S is usually
598 incorporated as sulfate rather than sulfide in the apatite structure (Peng et al. 1997;
599 Parrat et al. 2002; Parat and Holtz 2004). This is consistent with our data. Many of
600 the Gardar intrusions are known to have crystallized under reduced conditions
601 (Upton and Thomas 1980; Larsen and Sørensen 1987; Marks & Markl 2001). Redox
602 conditions during the crystallization of gabbros and many granitoids are generally
603 more oxidized. Also, the relatively high S contents in some of the Tamazeght rocks
604 are in line with relatively oxidized conditions in some lithologies (Marks et al. 2008).

605 The abundance of Si in apatite is highly variable in igneous rocks. The highest
606 concentrations are observed in carbonatites and the Ilímaussaq agpaites. Obviously
607 the Si contents in apatites do not reflect the Si-contents of the host melts as apatites
608 from granitic rocks are generally relatively low in Si (**Fig. 9d**). This can be explained
609 by the often observed coupled substitution $Ca^{2+} + P^{5+} \leftrightarrow REE^{3+} + Si^{4+}$ (see above)
610 linking REE with Si contents in apatite (Pan and Fleet 2002; Fleet et al. 2000; Zirner
611 et al. 2015; Rønsbo 1989; 2008).

612

613 **Ca-Fe-Mn systematics –** There is no clear relationship between the Fe-content of
614 the apatites and that of their host rock (**Fig. 9**). Apatite Mn contents are known to be
615 relatively high in muscovite-bearing granites. This has been related to their source

616 composition and redox conditions during apatite crystallization (Sha and Chappell
617 1999; Belousova et al. 2002). Recently, a negative correlation between Mn in apatite
618 and oxygen fugacity (f_{O2}) was proposed as a potential oxybarometer (Miles et al.
619 2014). Therefore it is surprising that Mn contents in strongly reduced rocks of the
620 Gardar Province are exceptionally low (mostly below 500 µg/g) as opposed to
621 muscovite-bearing granites, where apatite may contain Mn at the wt%-level (e.g.,
622 Sha and Chappell 1999; Belousova et al. 2002; Teiber et al. 2014; 2015a). We
623 suggest that this is because of the strong temperature-dependence of f_{O2} (e.g.,
624 Huebner 1971; Ohmoto and Kerrick 1977). Thus, reduced conditions may result in
625 high Mn contents in apatite that crystallized at relatively low temperatures (as
626 observed in some muscovite-bearing granites) or in low Mn contents, if apatite
627 crystallized at relatively high temperatures, as is the case in many syenitic rocks.
628 Therefore redox or temperature estimates based on the Mn content of apatite are
629 only possible if combined with independent estimates on T or f_{O2}.

630

631 **F-Cl-OH systematics -** In most igneous rocks, apatite almost invariably comprises
632 fluorapatite-hydroxylapatite solid solutions. Apatites with significant amounts of Cl
633 approaching chlorapatite composition are known only from some relative primitive
634 rocks such as gabbros and diorites (**Fig. 9c**). This could either relate to source
635 composition (cf. Sha and Chappell 1999; Teiber et al. 2014) or to the changing
636 partitioning behavior of F and Cl between apatite and melt/fluid at variable
637 crystallization temperatures (e.g., Mathez and Webster 2005; Webster et al. 2009;
638 Patino Douce et al. 2011; Doherty et al. 2014). Interpretion of the significance of the
639 hydroxylapatite component is hampered by analytical difficulties. Since most
640 published apatite analyses are based on EMPA data, OH is generally calculated on

the basis of stoichiometry on the halogen site. Only recently has direct space-resolved analysis of H in apatite has become possible by means of SIMS techniques (e.g., Boyce and Hervig 2008; McCubbin et al. 2010). Even if EMPA analyses are performed using appropriate conditions that avoid migration of F and Cl during analysis (Goldoff et al. 2012; Stormer et al. 1993; Wang et al. 2014), the potential incorporation of the carbonate anion complex is generally neglected. Relatively few studies of carbon in apatite are available, mostly from carbonatitic rocks (e.g. Sommerauer and Katz-Lehnert 1985; Binder and Troll 1989; Santos and Clayton 1995; Nadeau et al. 1999) and apatite from the lithospheric mantle (O'Reilly and Griffin 2000). Recent data (Riker et al. 2014), however, imply that CO_2 may behave compatibly in apatite such that carbonate might be an important component in apatite from various igneous rocks.

Implications

Apatites from alkaline rock suites can contain exceptionally high levels of REE, Si, and Sr that exceed even those in carbonatites. This is attributed to a combination of an enriched source composition and the early magmatic differentiation history. At the same time they are generally (but not always) poor in Fe, Mn, and S as a result of the usually reduced character of the melts that they grew in relatively high temperatures.

Most of the observed compositional variation is caused by two coupled substitutions involving Na, REE, Si, Ca and P, namely $Ca^{2+} + P^{5+} \leftrightarrow REE^{3+} + Si^{4+}$ and $2Ca^{2+} \leftrightarrow REE^{3+} + Na^{+}$. Consequently REE and Si are considered as reliable petrogenetic indicators for fractional crystallization because potential redistribution processes are minimized by the slow diffusion of Si and REE through the apatite. In contrast, Na (and Sr) are prone to diffusive redistribution because of their rapid diffusion in apatite,

666 which diminishes their usefulness as petrogenetic indicators in alkaline plutonic
667 complexes.

668

669 **Acknowledgments -** We acknowledge discussions with Ralf Halama, Johannes
670 Schönenberger and Holger Teiber and funding by the Deutsche
671 Forschungsgemeinschaft (grant MA 2563/3-1). We highly appreciate the detailed
672 comments provided by Jim Webster and one anonymous reviewer and the editorial
673 handling of Dan Harlov.

674

675 # References cited

676 Allaart, J.H. (1976) Ketilidian mobile belt in South Greenland. In A. Escher and W.S.
677 Watt, W.S., Eds., Geology of Greenland, Grønlands Geologiske
678 Undersøgelse, 121-151.

679 Armstrong, J.T. (1991) Quantitative elemental analysis of individual microparticles
680 with electron beam instruments. In K.F.J. Heinrich and D.E. Newbury, Eds.,
681 Electron Probe Quantitation. New York & London, Plenum Press, 261-315.

682 Arzamastsev, A.A., Bea, F., Glaznev, V.N., Arzamastseva, L.V., and Montero, P.
683 (2001) Kola alkaline province in the Paleozoic: evaluation of primary mantle
684 magma composition and magma generation conditions. Russian Journal of
685 Earth Sciences, 3, 1-32.

686 Ayers, J.C., and Watson, E.B. (1993) Apatite/fluid partitioning of rare-earth elements
687 and strontium: experimental results at 1.0 GPa and 1000 °C and application to
688 models of fluid-rock interaction. Chemical Geology, 110, 299-314.

689 Bailey, J.C., Gwozdz, R., Rose-Hansen, J., and Sørensen, H. (2001) Geochemical
690 overview of the Ilimaussaq alkaline complex, South Greenland. Geology of
691 Greenland Survey Bulletin, 190, 35-53.

692 Belousova, E.A., Griffin, W.L., O´Reilly, S.Y., and Fisher, N.I. (2002) Apatite as an
693 indicator mineral for mineral exploration: trace-element composition and their
694 relationship to host rock type. Journal of Geochemical Exploration, 76, 45-69.

695 Belousova, E.A., Walters, S., Griffin, W.L., and O´Reilly, S.Y. (2001) Trace element
696 signatures of apatites from granitoids of Mount Isa Inlier, north-west
697 Queensland, Australia. Australian Journal of Earth Sciences, 48, 603-619.

698 Binder, G., and Troll, G. (1989) Coupled anion substitution in natural carbon-bearing
699 apatites. Contributions to Mineralogy and Petrology, 101, 394-401.

700 Blaxland, A.B., van Breemen, O., Emeleus, C.H., and Anderson, J.G. (1978) Age and
701 origin of the major syenite centers in the Gardar province of south Greenland:
702 Rb-Sr studies. Bulletin of the Geological Society of America, 89, 231-244.

703 Boudreau, A.E., Love, C., and Hoatson, D.M. (1993) Variation in the composition of
704 apatite in the Munni Munni Complex and associated intrusions of the West
705 Pilbara Block, Western Australia. Geochimica et Cosmochimica Acta, 57,
706 4467-4477.

707 Boyce, J.W., and Hervig, R.L. (2008) Magmatic degassing histories from apatite
708 volatile stratigraphy. Geology, 36, 63-66.

709 Bridgwater, D. (1967) Feldspathic inclusions in the Gardar igneous rocks of South
710 Greenland and their relevance to the formation of major Anorthosites in the
711 Canadian Shield. Canadian Journal of Earth Sciences, 4, 995-1014.

712 Bridgwater, D., and Coe, K. (1970) The role of stoping in the emplacement of the
713 giant dikes of Isortoq, South Greenland. Geological Journal, Special issue, 2,
714 67-78.

715 Bridgwater, D., and Harry, W.T. (1968) Anorthosite xenoliths and plagioclase
716 megacrysts in Precambrian intrusions of South Greenland. Meddelelser om
717 Grønland, 185 1-243.

718 Chakhmouradian, A., Reguir, E.P., and Mitchell, R.H. (2002) Strontium-apatite: New
719 occurrences, and the extent of Sr-for-Co substitution in apatite-group minerals.
720 The Canadian Mineralogist, 40, 121-136.

721 Cherniak, D.J. (2000) Rare earth element diffusion in apatite. Geochimica et
722 Cosmochimica Acta, 64, 3871-3885.

723 Cherniak, D.J., and Ryerson, F.J. (1993) A study of strontium diffusion in apatite
724 using Rutherford backscattering spectroscopy and ion implantation.
725 Geochimica et Cosmochimica Acta, 57, 4653-4662.

726 Chu, M.-F., Wang, K.-L., Griffin, W.L., Chung, S.-L., O´Reilly, S.Y., Pearson, N.J.,
727 and Ilzuka, Y. (2009) Apatite composition: Tracing petrogenetic processes in
728 Transhimalayan granitoids. Journal of Petrology, 50, 1829-185.

729 Dempster, T.J., Jolivet, M., Tubrett, M.N., and Braithwaite, C.J.R. (2003) Magmatic
730 zoning in apatite: a monitor of porosity and permeability change in granites.
731 Contributions to Mineralogy and Petrology, 145, 568-577.

732 Doherty, A.L., Webster, J.D., Goldoff, B.A., and Piccoli, P.M. (2014) Partitioning
733 behavior of chlorine and fluorine in felsic melt-fluid(s)-apatite systems at
734 50MPa and 850-950 °C. Chemical Geology, 384, 94-111.

735 Emeleus, C.H. (1964) The Grønnedal-Ika alkaline complex, South Greenland. The
736 structure and geological history of the complex. Meddelelser om Grønland,
737 172, 1-75.

738 Escher, A., and Watt, W.S. (1976) Geology of Greenland. Geological Survey of
739 Greenland, 603.

740 Ferguson, J. (1964) Geology of the Ilimaussaq alkaline intrusion, South Greenland.
741 Bulletin Grønlands Geologiske Undersøgelse, 39, 82.

742 Finch, A.A., Mansfeld, J., and Andersen, T. (2001) U-Pb radiometric age of Nunarsuit
743 pegmatite, Greenland: constraints on the timing of Gardar magmatism.
744 Bulletin of the Geological Society of Denmark, 48, 1-7.

745 Fleet, M.E., Liu, X., and Pan, Y. (2000) Site preference of Rare Earth Elements in
746 hydroxyapatite. Journal of Solid State Chemistry, 149, 391-398.

747 Garde, A.A., Hamilton, M.A., Chadwick, B., Grocott, J., and McCaffrey, K.J.W. (2002)
748 The Ketilidian orogen of South Greenland: geochronology, tectonics,
749 magmatism, and fore-arc accretion during Palaeoproterozoic oblique
750 convergence. Canadian Journal of Earth Sciences, 39, 765-793.

751 Giehl, C., Marks, M.A.W., and Nowak, M. (2012) Phase relations and liquid lines of
752 descent of an iron-rich peralkaline phonolitic melt: en experimental study.
753 Contributions to Mineralogy and Petrology, 165, 283-304.

754 Goldoff, B., Webster, J.D., and Harlov, D.E. (2012) Characterization of fluor-
755 chlorapatites by electron probe microanalysis with a focus on time-dependent
756 intensity variation of halogens. The American Mineralogist, 97, 1103-1115.

757 Halama, R., Marks, M., Brügmann, G.E., Siebel, W., Wenzel, T., and Markl, G.

(2004) Crustal contamination of mafic magmas: evidence from a petrological, geochemical and Sr-Nd-Os-O isotopic study of the Proterozoic Isortoq dike swarm, South greenland. Lithos, 74, 199-232.

Halama, R., Vennemann, T., Siebel, W., and Markl, G. (2005) The Grønnedal-Ika carbonatite-syenite complex, south Greenland: Carbonatite fromation by liquid immiscibility. Journal of Petrology, 46, 191-217.

Halama, R., Waight, T., and Markl, G. (2002) Geochemical and isotopic zoning patterns of plagioclase megacrysts in gabbroic dikes from the Gardar Province, South Greenland: implications for crystallisation processes in anorthositic magmas. Contributions to Mineralogy and Petrology, 144, 109-127.

Halama, R., Wenzel, T., Upton, B.G.J., Siebel, W., and Markl, G. (2003) A geochemical and Sr-Nd-O isotopic study of the Proterozoic Eriksfjord Basalts, Gardar Province, South Greenland: Reconstruction of an OIB-signature in crustally contaminated rift-related basalts. Mineralogical Magazine, 67, 831-853.

Hammouda, T., Chantel, J., and Devidal, J.-L. (2010) Apatite solibility in carbonatitic liquids and trace element partitioning between apatite and carbonatite at high pressure. Geochimica et Cosmochimica Acta, 74, 7220-7235.

Harlov, D., and Förster, H.J. (2003) Fluid-induced nucleation of (Y+REE)-phosphate minerals within apatite: Nature and experiment. Part II. Fluorapatite. The American Mineralogist, 88, 1209-1229.

Harlov, D., Wirth, D., and Förster, H.J. (2005) An experimental study of dissolution-reprecipitation in fluorapatite: fluid infiltration and the formation of monazite.

Contributions to Mineralogy and Petrology, 150, 268-286.

Harlov, D., Wirth, D., and Hetherington, C.J. (2011) Fluid-mediated partial alteration in monazite: the role of coupled dissolution-reprecipitation in element redistribution and mass transfer. Contributions to Mineralogy and Petrology, 162, 329-348.

Henderson, C.M.B., and Pierozynski, W.J. (2012) An experimental study of Sr, Ba and Rb partitioning between alkali feldspar and silicate liquids in the system nepheline-kalsilite-quartz at 0.1 GPa P(H_2O): a revisitation and reassessment. Mineralogical Magazine, 76, 157-190.

Hinton, R.W., and Paterson, B. (1994) Crystallisation history of granitic magma: Evidence from trace element zoning. Mineralogical Magazine, 58, 416-417.

Hoskin, P.W.O., Kinny, P.D., Wyborn, D., and Chappell, B.W. (2000) Identifying accessory mineral saturation during differentiation in granitoid magmas: an integrated approach. Journal of Petrology, 41, 1365-1396.

Huebner, J.S. (1971) Buffering techniques for hydrostatic systems at elevated pressure. In G.C. Ulmer, Ed., Springer, Berlin, 123-177.

Joliff, B.L., Papike, J.J., Shearer, C.K., and Shimizu, N. (1989) Inter- and intra-crystal REE variations in apatite from the Bob Ingersoll pegmatite, Black Hills, South Dakota. Geochimica et Cosmochimica Acta, 53, 429-441.

Jones, A.P. (1980) The petrology and structure of the Motzfeld centre, Igaliko, south Greenland. PhD thesis, University of Durham.

Jones, A.P., and Larsen, L.M. (1985) Geochemistry and REE minerals of nepheline syenites from the Motzfeld centre, south Greenland. The American

Mineralogist, 70, 1087-1100.

Kramm, U., and Kogarko, L.N. (1994) Nd and Sr isotope signatures of the Khibina and Lovozero agpaitic centres, Kola Province, Russia. Lithos, 32, 225-242.

Krumrei, T.V., Villa, I.M., Marks, M.A.W., and Markl, G. (2006) A $^{40}Ar/^{39}Ar$ and U/Pb isotopic study of the Ilimaussaq complex, South Greenland: Implications for the ^{40}K decay constant and for the duration of magmatic activity in a peralkaline complex. Chemical Geology, 227, 258-273.

Larsen, J.G. (1977) Petrology of the late lavas of the Eriksfjord Formation, Gardar province, South Greenland. Bulletin Grønlands Geologiske Undersøgelse, 125, 1-31.

Larsen, L.M., and Sørensen, H. (1987) The Ilimaussaq intrusion-progressive crystallization and formation of layering in an agpaitic magma. In J.G. Fitton and B.G.J. Upton, Eds., Alkaline igneous rocks, Geological Society of London, Special Publication, 30, 473-488.

Larsen, L.M., and Steenfelt, A. (1974) Alkali loss and retention in an iron-rich peralkaline phonolite dike from the Gardar province, south Greenland. Lithos, 7, 81-90.

Liferovich, R.P., and Mitchell, J.G. (2006) Apatite-group minerals from nepheline syenite, Pilansberg alkaline complex, South Africa. Mineralogical Magazine, 70, 463-484.

Marks, M., Halama, R., Wenzel, T., and Markl, G. (2004b) Trace element variations in clinopyroxene and amphibole from alkaline to peralkaline syenites and granites: implications for mineral-melt trace-element partitioning. Chemical

828 Geology, 211, 185-215.

829 Marks, M., and Markl, G. (2001) Fractionation and assimilation processes in the
830 alkaline augite syenite unit of the Ilimaussaq Intrusion, South Greenland, as
831 deduced from phase equilibria. Journal of Petrology, 42, 1947-1969.

832 -. (2003) Ilimaussaq 'en miniature': closed-system fractionation in an agpaitic dike
833 rock from the Gardar province, south Greenland. Mineralogical Magazine, 67,
834 893-919.

835 -. (2015) The Ilimaussaq alkaline complex, South Greenland. In: Charlier, B., Namur,
836 O., Latypov, R., Tegner, C. (eds.) Layered Intrusions, pp.649-691. Springer
837 Geology, Dordrecht. 649-691.

838 Marks, M., Vennemann, T., Siebel, W., and Markl, G. (2004a) Nd-, O-, and H-isotopic
839 evidence for complex, closed-system fluid evolution of the peralkaline
840 Ilimaussaq Intrusion, South Greenland. Geochimica et Cosmochimica Acta,
841 68, 3379-3395.

842 Marks, M., Vennemann, T.W., Siebel, W., and Markl, G. (2003) Quantification of
843 magmatic and hydrothermal processes in a peralkaline syenite- alkali granite
844 complex based on textures, phase equilibria, and stable and radiogenic
845 isotopes. Journal of Petrology, 44, 1247-1280.

846 Marks, M.A.W., Hettmann, K., Schilling, J., Frost, B.R., and Markl, G. (2011) The
847 mineralogical diversity of alkaline igneous rocks: Critical factors for the
848 transition from miaskitic to agpaitic phase assemblages. Journal of Petrology,
849 52, 439-455.

850 Marks, M.A.W., and Markl, G. (in press) The Ilímaussaq alkaline complex, South

Greenland. In B. Charlier, O. Namur, R. Latypov, and C. Tegner, Eds., Layered Intrusions. Springer, Dordrecht.

Marks, M.A.W., Rudnick, R., Vennemann, T., McCammon, C., and Markl, G. (2007) Arrested kinetic Li isotope fractionation at the margin of the Ilimaussaq complex, South Greenland: evidence for open-system processes during final cooling of peralkaline igneous rocks. Chemical Geology, 246, 207-230.

Marks, M.A.W., Schilling, J., Coulson, I.M., Wenzel, T., and Markl, G. (2008) The alkaline-peralkaline Tamazeght complex, High Atlas Mountains, Morocco: Mineral chemistry and petrological constraints for derivation from a compositionally heterogeneous mantle source. Journal of Petrology, 49, 1097-1131.

Marks, M.A.W., Wenzel, T., Whitehouse, M., Loose, M., Zack, T., Barth, M., Worgard, L., Krasz, V., Eby, G.N., Stosnach, H., and Markl, G. (2012) The volatile inventory (F, Cl, Br, S, C) of magmatic apatite: An integrated analytical approach. Chemical Geology, 291, 241-255.

Mathez, E.A., and Webster, J.D. (2005) Partitioning behavior of chlorine and fluorine in the system apatite-silicate melt-fluid. Geochimica et Cosmochimica Acta, 69, 1275-1286.

McCreath, J.A., Finch, A.A., Simonsen, S.L., Donaldson, C.H., and Armour-Brown, A. (2012) Independent ages of magmatic and hydrothermal activity in alkaline igneous rocks: The Motzfeld centre, Gardar Province, south Greenland. Contributions to Mineralogy and Petrology, 163, 967-982.

McCubbin, F.M., Steele, A., Hauri, E.H., Nekvasil, H., Yamahita, S., and Hemley, R.J. (2010) Nominally hydrous magmatism on the moon. Proceedings of the

National Academy of Sciences of the United States of America, 107, 11223-11228.

Miles, A.J., Graham, C.M., Hawkesworth, C., Gillespie, M.R., Hinton, R.W., and Bromiley, G.D. (2014) Apatite: A new redox proxy for silicic magmas? Geochimica et Cosmochimica Acta, 132, 101-119.

Nadeau, S.L., Epstein, S., and Stolper, E. (1999) Hydrogen and carbon abundances and isotopic ratios in apatite from alkaline intrusive complexes, with a focus on carbonatites. Geochimica et Cosmochimica Acta, 63, 1837-1851.

Nash, W.P. (1984) Phosphate minerals in terrestrial igneous and metamorphic rocks. In J. Nriagu and P. Moore, Eds., Phosphate Minerals. Springer, Berlin., 215-241.

Ohmoto, H., and Kerrick, D. (1977) Devolatization equilibria in graphitic systems. American Journal of Science, 277, 1013-1044.

O'Reilly, S.Y., and Griffin, W.L. (2000) Apatite in the mantle: implications for metasomatic processes and high heat production in Phanerozoic mantle. Lithos, 53, 217-232

Pan, Y., and Fleet, M.E. (2002) Compositions of the apatite-group minerals: substitution mechanisms and controlling factors. Reviews in Mineralogy and Geochemistry, 48, 13-49.

Parat, F., Dungan, M.A., and Streck, M.J. (2002) Anhydrite, pyrrhotite and sulfur-rich apatite: tracing sulfur evolution of an Oligocene andesite (Eagle Mountain, Colorado, U.S.A.). Lithos, 64, 63-75.

Parat, F., and Holtz, F. (2004) Sulfur partitioning between apatite and melt and effect

of sulfur on apatite sulibility at oxidizing conditions. Contributions to Mineralogy and Petrology, 147, 201-212.

Parsons, I. (1972) Petrology of the Puklen syenite-alkali granite complex, Nunarssuit, South Greenland. Meddelelser om Grønland, 195, 1-73.

Pasero, M., Kampf, A.R., Roden, M.F., Chaumba, J., fleisher, C., and Yogodzinski, G. (2011) Nomenclature of the apatite supergroup minerals. European Journal of Mineralogy, 22, 163-179.

Patino Douce, A.E., Roden, M.F., Chaumba, J., Fleisher, C., and Yogodzinski, G. (2011) Compositional variability of terrestrial mantle apatites, thermodynamic modeling of apatite volatile contents, and the halogen and water budgets of planetary mantles. Chemical Geology, 288, 14-31.

Peng, G., Luhr, J.F., and McGee, J. (1997) Factors controlling sulfur concentrations in volcanic apatite. The American Mineralogist, 82, 1210-1224.

Petersen, O.V. (2001) List of minerals identified in the Ilimaussaq alkaline complex, South Greenland. Geology of Greenland Survey Bulletin, 190, 25-34.

Piccoli, P.M., and Candela, P.A. (2002) Apatite in igneous systems. Reviews in Mineralogy and Geochemistry, 48, 255-292.

Poulsen, V. (1964) The sandstones of the Precambrian Eriksfjord Formation in South Greenland. Rapport Grønlands Geologiske Undersøgelse, 2, 16.

Prowatke, S., and Klemme, S. (2006) Trace element partitioning between apatite and silicate melts. Geochimica et Cosmochimica Acta, 70, 4513-4527.

Pulvertaft, T.C.R. (1961) The Puklen intrusion, Nunarssuit, SW Greenland. Meddelelser om Grønland, 123, 35-49.

Rae, D.A., Coulson, I.M., and Chambers, A.D. (1996) Metasomatism in the North Qoroq centre, South Greenland; apatite chemistry and rare-earth element transport. Mineralogical Magazine, 60, 207-220.

Reid, J.B., Evans, O.C., and Fates, D.G. (1983) Magma mixing in granitic rocks of the central Sierra Nevada, California. Earth and Planetary Science Letters, 66, 243-261.

Riker, J.M., M.C.S. Humphreys, and R.A. Brooker (2014) Apatite as a tool for tracking magmatic CO_2 contents. Abstract V12A-02, 2014 Fall Meeting, AGU, San Francisco.

Rønsbo, J.G. (1989) Coupled substitutions involving REEs and Na and Si in apatites in alkaline rocks from the Ilímaussaq intrusion, South Greenland, and the petrological implications. The American Mineralogist, 74, 896-901.

-. (2008) Apatite in the Ilimaussaq alkaline complex: Occurence, zonation and compositional variation. Lithos, 106, 71-82.

Santos, R.V., and Clayton, R.N. (1995) The carbonate content in high-temperature apatite: An analytical method applied to apatite from the Jacupiranga alkaline complex. The American Mineralogist, 80(336-344).

Schilling, J., Wu, F.-Y., McCammon, C., Wenzel, T., Marks, M.A.W., Pfaff, K., Jacob, D.E., and Markl, G. (2011) The compositional variability of eudialyte-group minerals. Mineralogical Magazine, 75, 87-115.

Schönenberger, J., and Markl, G. (2008) The magmatic and fluid evolution of the Motzfeld Intrusion in South Greenland: Insights into the formation of agpaitic and miskitic rocks. Journal of Petrology, 49, 1549-1577.

Seifert, W., Kämpf, H., and Wasternack, J. (2000) Compositional variation in apatite, phlogopite and other accessory minerals of the ultramafic Delitzsch complex, Germany: implications for cooling history of carbonatites. Lithos, 53, 81-100.

Sha, L.-K. (1995) Genesis of zoned hydrous ultramafic/mafic-silicic intrusive complexes: an MHFC hypothesis. Earth Science Reviews, 39, 59-90.

Sha, L.-K., and Chappell, B.W. (1999) Apatite chemical composition, determined by electron microprobe and laser-ablation inductively coupled plasma mass spectrometry, as a probe into granite petrogenesis. Geochimica et Cosmochimica Acta, 63, 3861-3881.

Shore, M., and Fowler, A.D. (1996) Oscillatory zoning in minerals; a common phenomenon. The Canadian Mineralogist, 34, 1111-1126.

Sommerauer, J., and Katz-Lehnert, K. (1985) A new partial substitution mechanism of CO_3^{2-}/CO_3OH^{3-} and SiO_4^{4-} for the PO_4^{3-} group in hydroxyapatite from the Kaiserstuhl alkaline complex (SW Germany). Contributions to Mineralogy and Petrology, 91, 360-368.

Sørensen, H. (1997) The agpaitic rocks - an overview. Mineralogical Magazine, 61, 485-498.

Sørensen, H., and Larsen, L.M. (2001) The hyper-agpaitic stage in the evolution of the Ilímaussaq alkaline cmplex, South Greenland. Geology of Greenland survey Bulletin, 190, 83-94.

Stevenson, R., Upton, B.G.J., and Steenfelt, A. (1997) Crust-mantle interaction in the evolution of the Ilimaussaq Complex, South Greenland: Nd isotopic studies. Lithos, 40, 189-202.

967 Stormer, J.C.J., Pierson, M.L., and Tacker, R.C. (1993) Variation in F and Cl X-ray
968 intensity due to anisotropic diffusion in apatite during electron microprobe
969 analysis. The American Mineralogist, 78, 641-648.

970 Streck, M.J. (2008) Mineral textures and zoning as evidence for open system
971 processes. Reviews in Mineralogy and Geochemistry, 69, 595-622.

972 Sweatman, T.R., and Long, J.V.P. (1969) Quantitative electron-probe microanalysis
973 of rock-forming minerals. Journal of Petrology, 10, 332-379.

974 Teiber, H., Marks, M.A.W., Arzamastsev, A., Wenzel, T., and Markl, G. (2015a)
975 Compositional variation in apatite from various host rocks: clues with regards
976 to source composition and crystallization conditions. Neues Jahrbuch fuer
977 Mineralogie Abhandlungen, 192, 151-167.

978 Teiber, H., Marks, M.A.W., Wenzel, T., Zack, T., Siebel, W., Altherr, R., and Markl, G.
979 (2014) The distribution of halogens (F, Cl, Br) in granitoid rocks. Chemical
980 Geology, 374-375, 92-109.

981 Teiber, H., Scharrer, M., Marks, M.A.W., Arzamastsev, A., Wenzel, T., and Markl, G.
982 (2015b) Equilibrium partitioning and subsequent re.distribution of halogens
983 among apatite-biotite-amphibole assemblages from mantle-derived plutonic
984 rocks: Complexitites revealed. Lithos, 220-223, 221-237.

985 Tepper, J.H., and Kuehner, S.M. (1999) Complex zoning in apatite from the Idaho
986 Batholith: a record of magma mixing and intracrystalline trace element
987 diffusion. The American Mineralogist, 84, 581-595

988 Upton, B.G.J. (2013) Tectono-magmatic evolution of the younger Gardar southern
989 rift, South Greenland. Geological Survery of Denmark and Greenland Bulletin,

29, 1-124.

Upton, B.G.J., and Emeleus, C.H. (1987) Mid-Proterozoic alkaline magmatism in southern Greenland: the Gardar province. In J.G. Fitton and B.G.J. Upton, Eds., Alkaline igneous rocks, Geological Society of London, Special Publication, 30, 449-471.

Upton, B.G.J., Emeleus, C.H., Heaman, L.M., Goodenough, K.M., and Finch, A. (2003) Magmatism of the mid-Proterozoic Gardar Province, South Greenland: chronology, petrogenesis and geological setting. Lithos, 68, 43-65.

Upton, B.G.J., MacDonald, R., Hill, P.G., Jeffereies, B., and Ford, C.E. (1976) Narsarsukite: a new occurrence in peralkaline trachyte, South Greenland. Mineralogical Magazine, 40, 737-746.

Upton, B.G.J., MacDonald, R., Odling, N., Rämö. O.T., and Baginski, B. (2013) Kungnat revisited: A review of five decades of research into an alkaline complex in south Greenland, with new trace element and Nd isotopic data. Mineralogical Magazine, 77, 523-550.

Upton, B.G.J., Stephenson, D., and Martin, A.R. (1985) The Tugtutôq older giant dike complex: mineralogy and geochemistry of an alkali gabbro-augite-syenite-foyaite association in the Gardar Province of South Greenland. Mineralogical Magazine, 49, 624-642.

Upton, B.G.J., and Thomas, J.E. (1980) The Tugtutôq younger giant dike complex, South Greenland: fractional crystallisation of transitional olivine basalt magma. Journal of Petrology, 21, 167-198.

Wang, L.-X., Marks, M.A.W., Wenzel, T., von der Handt, A., Keller, J., Teiber, H., and

Markl, G. (2014) Apatites from the Kaiserstuhl Volcanic Complex, Germany: new constraints on the relationship between carbonatite and associated silicate rocks. European Journal of Mineralogy, 26, 397-414.

Watson, E.B., and Green, T.H. (1981) Apatite/liquid partitioning coefficients for the rare earth elements and strontium. Earth and Planetary Science Letters, 56, 405-421.

Webster, J.D., Tappen, C.M., and Mandeville, C.W. (2009) Partitioning behavior of chlorine and fluorine in the system apatite-melt-fluid. II: Felsic silicate systems at 200 MPa. Geochimica et Cosmochimica Acta, 73, 559-581.

Wyllie, P.J., Cox, K.G., and Biggar, G. (1962) The habit of apatite in synthetic systems and igneous rocks. Journal of Petrology, 3, 238-243.

Zirner, A.L.K., Marks, M.A.W., Wenzel, T., Jacob, D.E., and Markl, G. (2015) Rare Earth Elements in apatite as a monitor of magmatic and metasomatic processes: the Ilímaussaq complex, South Greenland. Lithos, 228-229, 12-22.

Figure captions

Fig. 1: Geological sketch map of the Gardar Province (South Greenland), showing the studied locations (modified from Escher and Watt 1976).

Fig. 2: Whole-rock compositions of the studied sample material. Data from Baileys et al. (2001); Halama et al. (2004); (2005); Jones (1980), Larsen and Steenfelt (1974); Marks et al. (2003); (2007); Upton and Thomas (1980); and Upton et al. (1976); (1985).

Fig. 3: Apatite textures from the Gønnedal-Ika complex (BSE images), showing concentric and oscillatory zoning (a), rounded core textures (b and c), and irregular overgrowth textures (d). Mineral abbreviations are the same as in the Table 1.

Fig. 4: Apatite textures from the Motzfeld and Puklen complexes (BSE images), showing concentric and oscillatory zoning (a-c), patchy zoning (d), homogeneous grains (e), and irregular overgrowth textures (f). Mineral abbreviations are the same as in the Table 1.

Fig. 5: Compositional variation of apatites from the Gardar Province. Abbreviations: IGL = Igdlutalik, T(OGDC) = Tugtutôq; Older Giant Dike Complex, T(YGDC) = Tugtutôq, Younger Giant Dike Complex; ISQ = Isortoq dike swarm; GRI = Grønnedal-Ika complex; PUK = Puklen complex; MOF = Motzfeldt; NQ North Qôroq complex (Rae et al. 1996); KUT = Kûngnât complex; and ILM = Ilímaussaq complex (Rønsbo 1998; 2008; Zirner et al. 2015). Analyses from IGL, T(OGDC), T(YGDC) and KUT (gray symbols) derive from different analytical conditions (see description of methods). For each locality the investigated samples are shown from left to right by decreasing X_{Mg} of their whole-rock and their mafic mineral composition.

Fig. 6: Compositional zoning with respect to Ce, Na, Sr, and Si for apatites from the Grønnedal-Ika (1 and 2) and the Motzfeld complexes (3-5). Apatite crystal (4) shows a rounded core whilst all the other apatites are concentrically zoned. In the latter type

Ce, Na, and Si increase from core to rim, while Sr decreases. In apatite grain (4), however, Na and Sr deviate from this general rule.

Fig. 7: Halogen contents for apatites from the Gardar Province. Abbreviations are the same as in Fig. 5. For each locality, the investigated samples are shown from left to right by decreasing X_{Mg} of their whole-rock and their mafic mineral composition. Analyses from IGL, T(OGDC), T(YGDC), and KUT (gray symbols) derive from different analytical conditions (see description of methods). Therefore, the halogen concentrations should be interpreted with caution, due to the mobility of F and less so Cl during analyses, which was not considered at the time of their analysis.

Fig. 8: Variation of (Ca + P) versus (REE + Si) for the investigated apatites, indicating the importance of the two coupled subtitutions $Ca^{2+} + P^{5+} = REE^{3+} + Si^{4+}$ and $2Ca^{2+} = REE^{3+} + Na^{+}$. Note that REE represents EMPA data for La and Ce. (a) All apatites. (b) Apatites from the intrusive complexes of Kûngnât, Grønnedal-Ika, Puklen, Motzfeldt, and Ilímaussaq, which was includes data from Rønsbo (1989), (2008) and Zirner et al. (2015). (c) Apatites from the dike rocks of Isortoq and Tugtutôq. Note the change of scale in the three subfigures.

Fig. 9: Comparison of apatite compositions (on a molar basis) from alkaline rocks (a), carbonatites (b), gabbros and diorites (c), and granites (d). Data for alkaline rocks are from this study, Rae et al. (1996), Zirner et al. (2015), Liferovich and Mitchell (2006), and Wang et al. (unpublished). Fields for carbonatites, gabbros, diorites, biotite ±

amphibole granites, and muscovite granites are taken from the recent compilation of Teiber et al. (2015a).

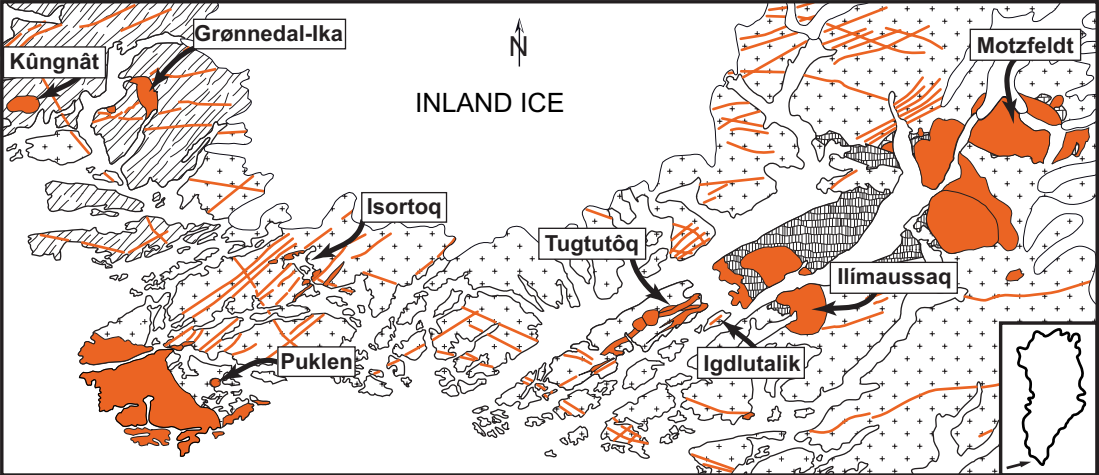

Ketilidian (Julianehåb batholith)

Archaean

0 10 20 30 km

Gardar sediments & volcanics (Eriksfjord Formation)

Gardar intrusive complexes

Gardar dyke rocks (schematic)

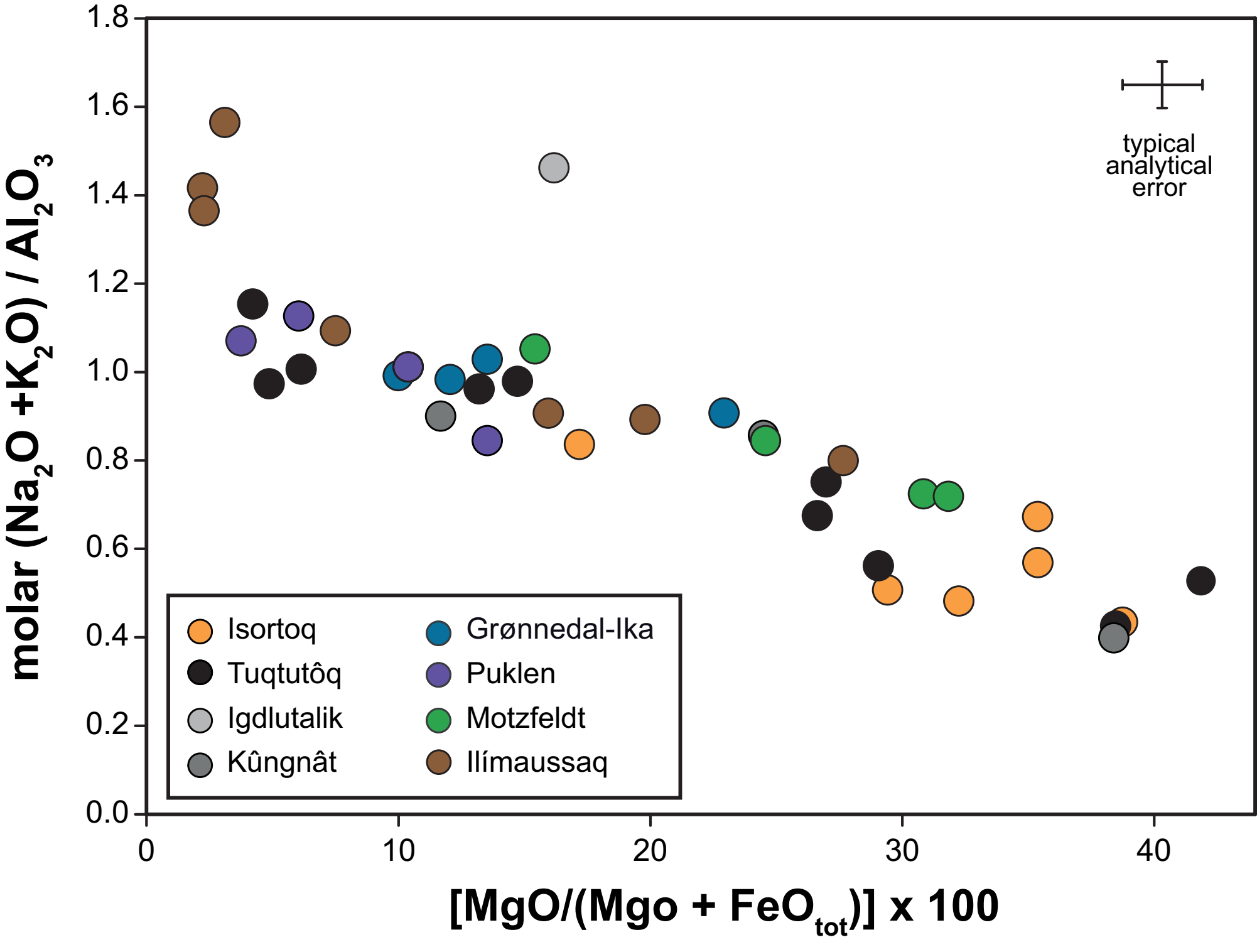
molar (Na2O +K2O) / Al2O3
[MgO/(Mgo + FeOtot)] x 100
typical analytical error
Isortoq
Tuqtutôq
Igdlutalik
Kûngnât
Grønnedal-Ika
Puklen
Motzfeldt
Ilímaussaq
0.0
0.2
0.4
0.6
0.8
1.0
1.2
1.4
1.6
1.8
0
10
20
30
40

Figure 3

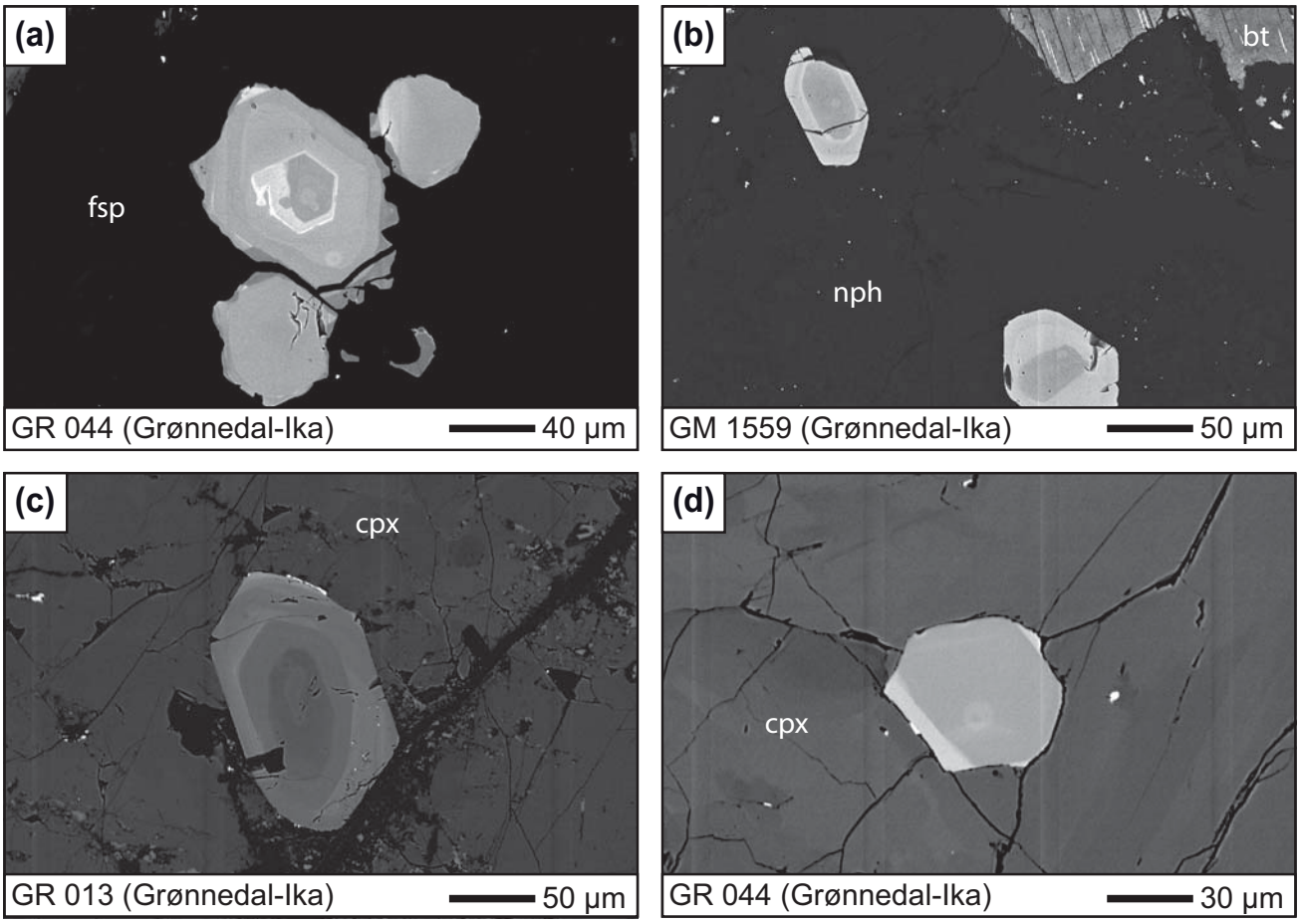
(a)
fsp
GR 044 (Grønnedal-Ika)
40 µm
(b)
bt
nph
GM 1559 (Grønnedal-Ika)
50 µm
(c)
cpx
GR 013 (Grønnedal-Ika)
50 µm
(d)
cpx
GR 044 (Grønnedal-Ika)
30 µm

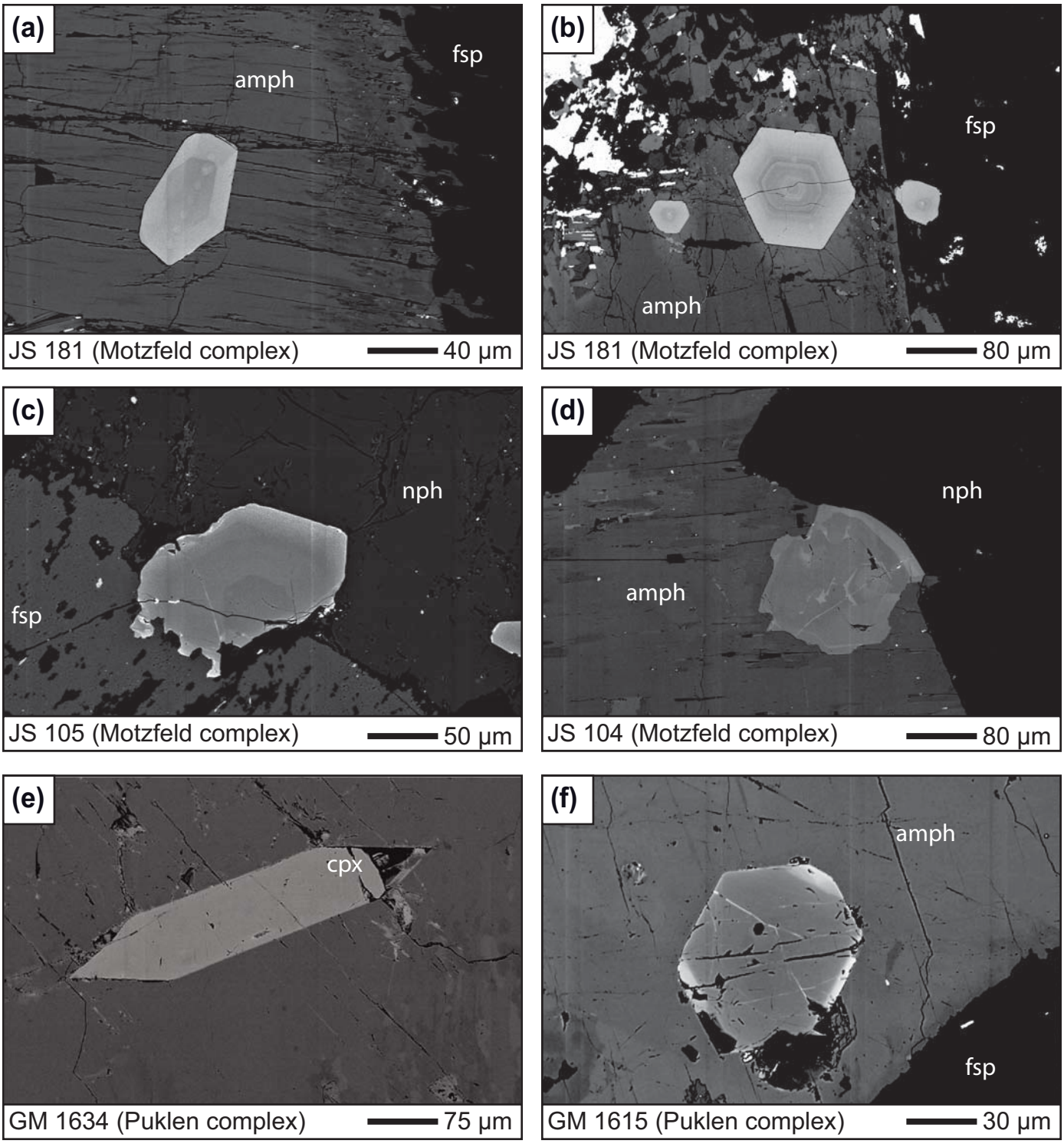
(a)
amph
fsp
JS 181 (Motzfeld complex)
40 µm
(b)
fsp
amph
JS 181 (Motzfeld complex)
80 µm
(c)
nph
fsp
JS 105 (Motzfeld complex)
50 µm
(d)
nph
amph
JS 104 (Motzfeld complex)
80 µm
(e)
cpx
GM 1634 (Puklen complex)
75 µm
(f)
amph
fsp
GM 1615 (Puklen complex)
30 µm

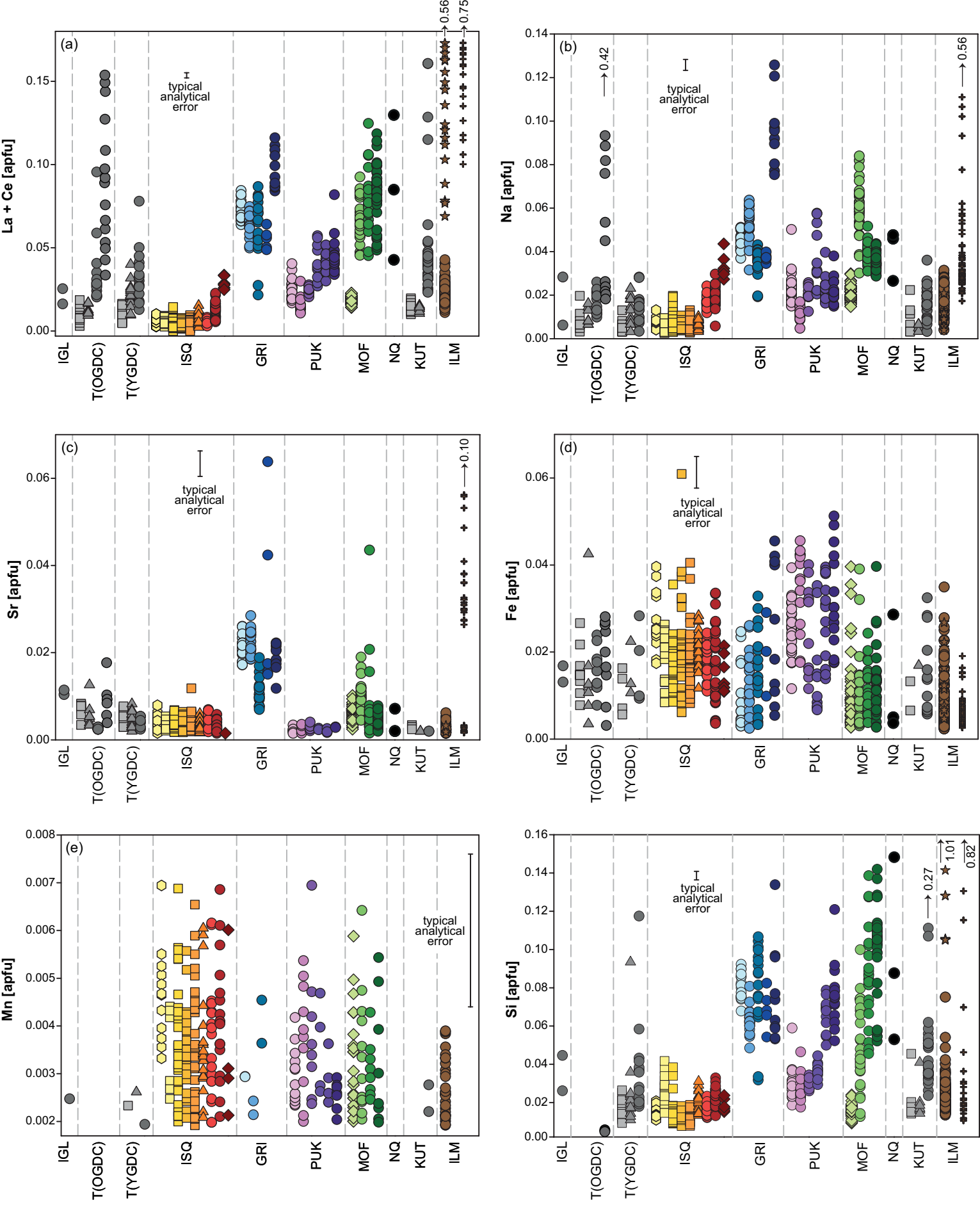
(a)
La + Ce [apfu]
typical analytical error
→ 0.56
→ 0.75
(b)
Na [apfu]
typical analytical error
→ 0.42
→ 0.56
(c)
Sr [apfu]
typical analytical error
→ 0.10
(d)
Fe [apfu]
typical analytical error
(e)
Mn [apfu]
typical analytical error
(f)
Si [apfu]
typical analytical error
→ 0.27
→ 1.01
→ 0.82
IGL
T(OGDC)
T(YGDC)
ISQ
GRI
PUK
MOF
NQ
KUT
ILM
anorthosite xenolith
gabbro
syenogabbro
larvikite
miaskitic syenite, pulaskite and foyaite
miaskitic syenite (secondary overgrowth)
agpaitic syenite

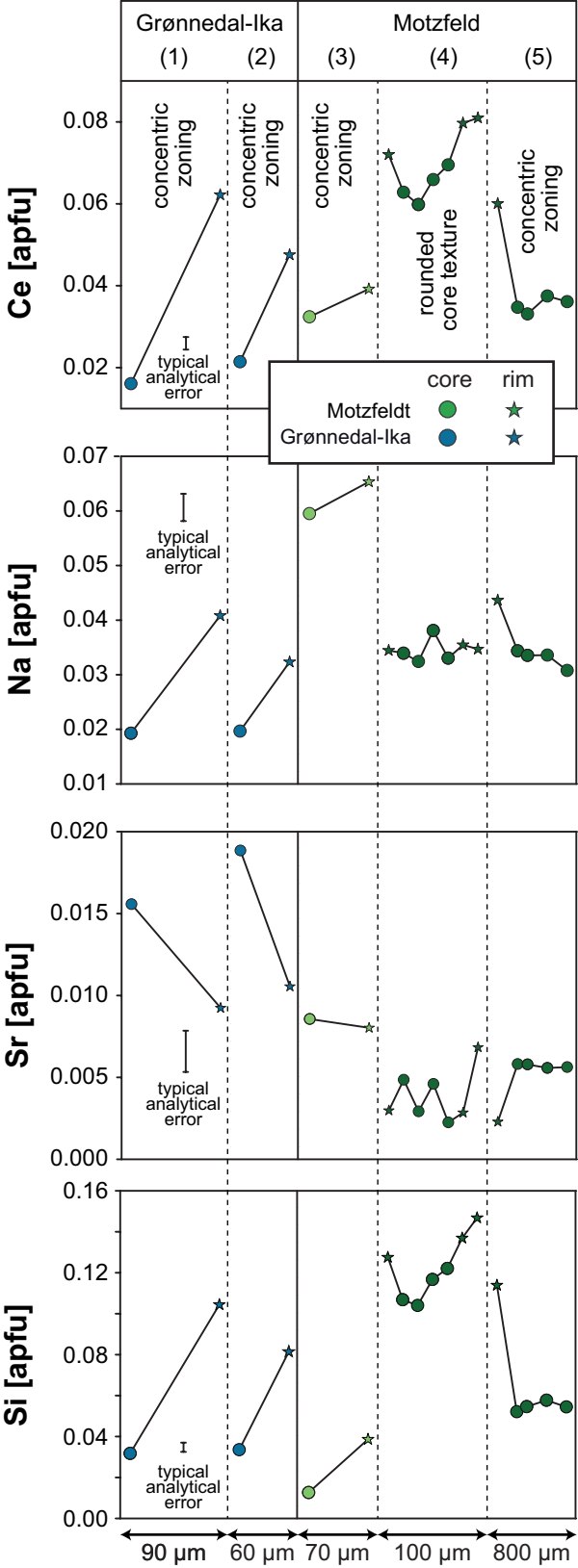
Grønnedal-Ika
(1)
(2)
Motzfeld
(3)
(4)
(5)
Ce [apfu]
Na [apfu]
Sr [apfu]
Si [apfu]
concentric zoning
rounded core texture
typical analytical error
core
rim
Motzfeldt
Grønnedal-Ika
90 µm
60 µm
70 µm
100 µm
800 µm

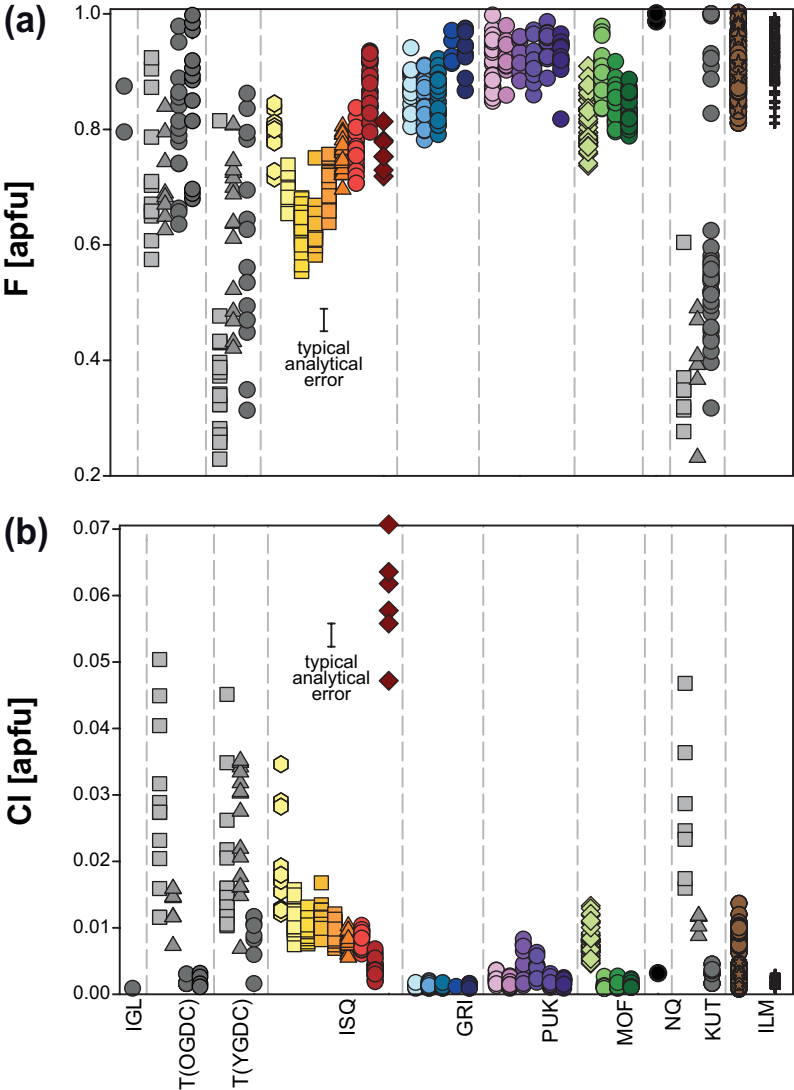
(a)
F [apfu]
1.0
0.8
0.6
0.4
0.2
typical analytical error
(b)
CI [apfu]
0.07
0.06
0.05
0.04
0.03
0.02
0.01
0.00
typical analytical error
IGL
T(OGDC)
T(YGDC)
ISQ
GRI
PUK
MOF
NQ
KUT
ILM

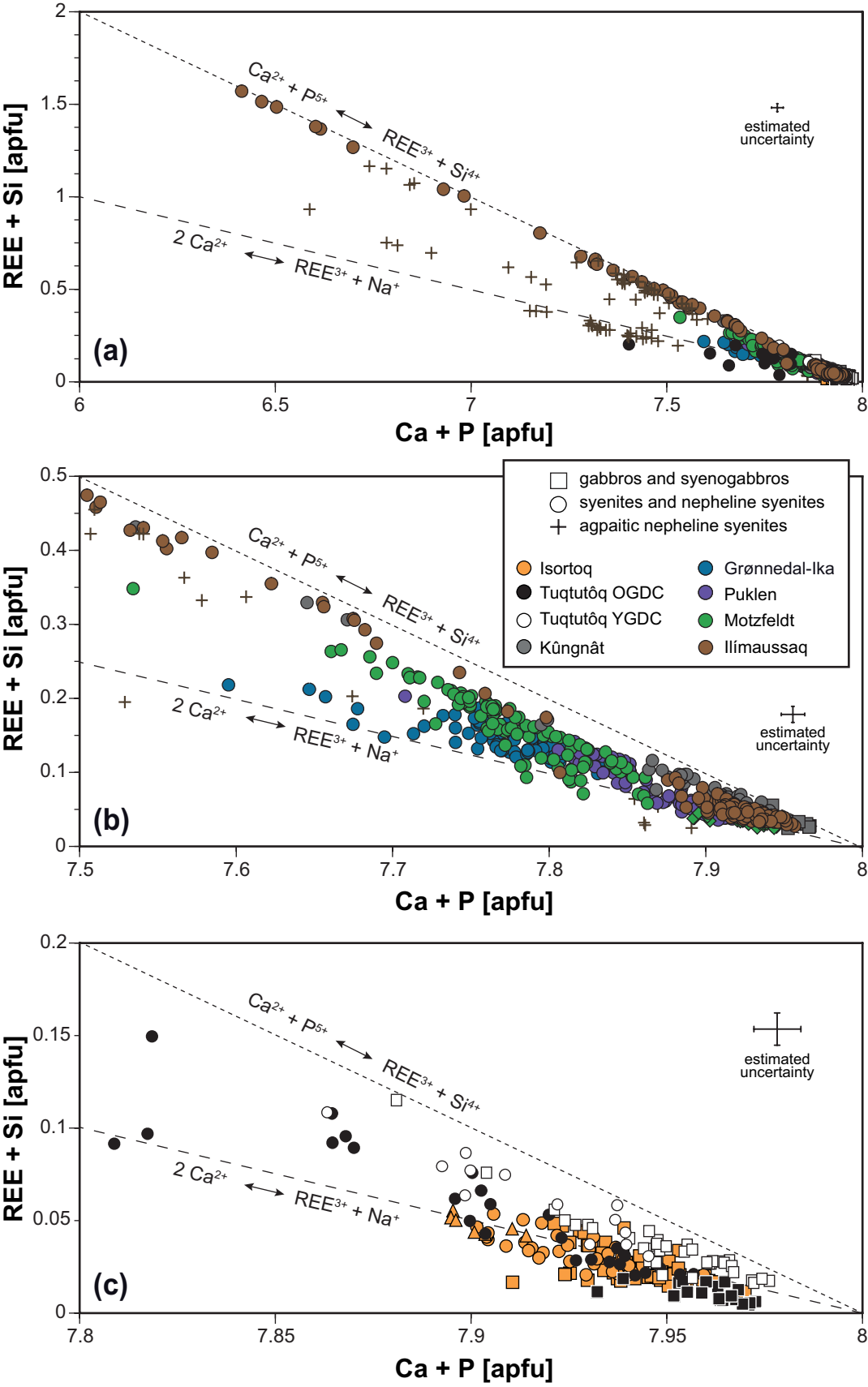
REE + Si [apfu]
Ca + P [apfu]
Ca2+ + P5+
REE3+ + Si4+
2 Ca2+
REE3+ + Na+
estimated uncertainty
(a)
(b)
(c)
gabbros and syenogabbros
syenites and nepheline syenites
agpaitic nepheline syenites
Isortoq
Tuqtutôq OGDC
Tuqtutôq YGDC
Kûngnât
Grønnedal-Ika
Puklen
Motzfeldt
Ilímaussaq

Figure 9

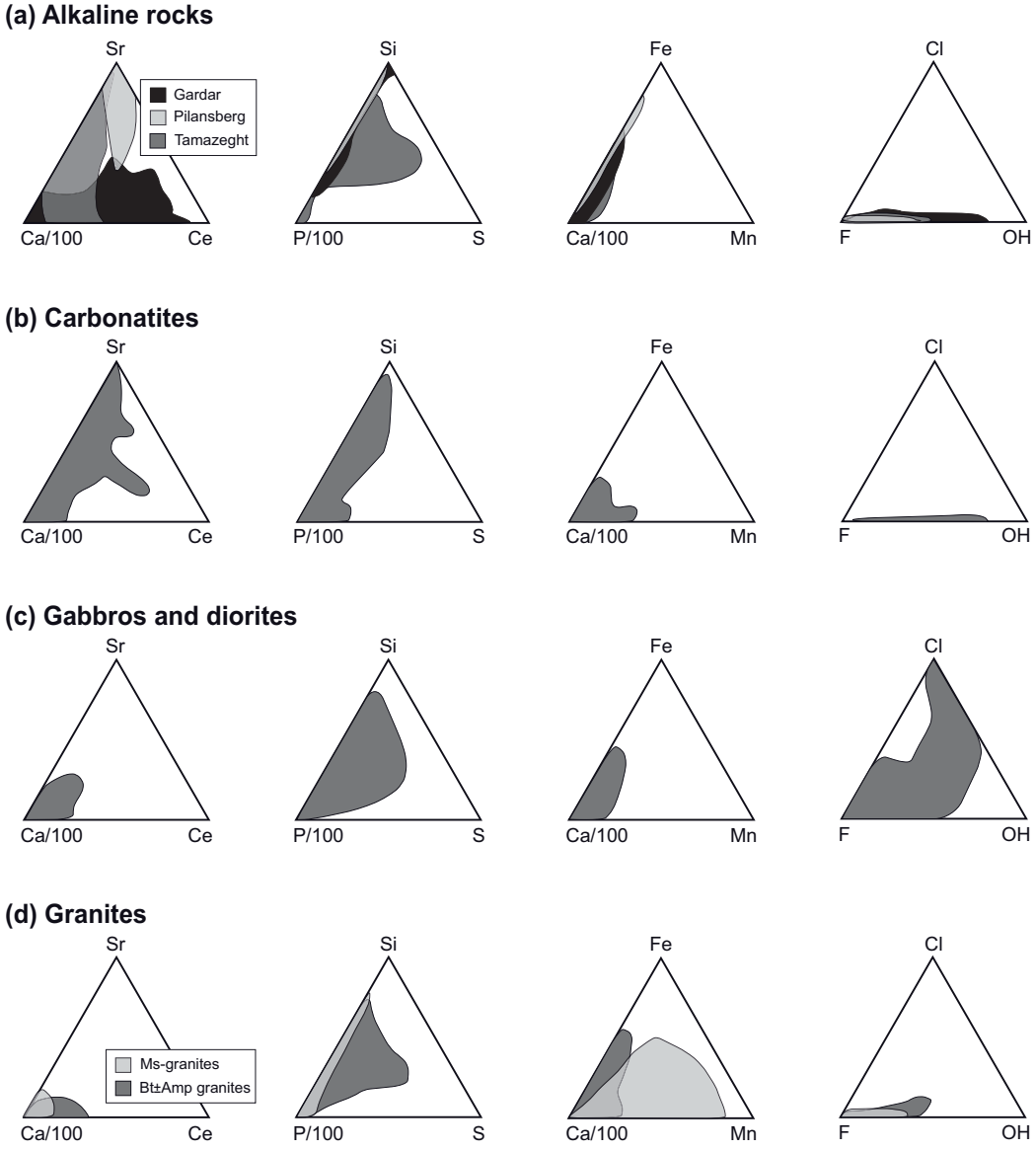
(a) Alkaline rocks
Sr
Si
Fe
Cl
Gardar
Pilansberg
Tamazeght
Ca/100
Ce
P/100
S
Ca/100
Mn
F
OH
(b) Carbonatites
Sr
Si
Fe
Cl
Ca/100
Ce
P/100
S
Ca/100
Mn
F
OH
(c) Gabbros and diorites
Sr
Si
Fe
Cl
Ca/100
Ce
P/100
S
Ca/100
Mn
F
OH
(d) Granites
Sr
Si
Fe
Cl
Ms-granites
Bt±Amp granites
Ca/100
Ce
P/100
S
Ca/100
Mn
F
OH

Table 1: Overview of the samples considered in this study, including their major mineralogy.

locality	sample	rock type	major minerals											
			Ol	Cpx	Amp	Pl	Afs	Nph	Qtz	Bt	Ox	Aen	Sod	Eud
Grønnedal-Ika	GR 044	nepheline syenite		x			x	x			x			
	GM 1559	nepheline syenite		x			x	x		x	x			
	GR 013	nepheline syenite		x			x	x			x			
	GR 001	nepheline syenite		x			x	x			x			
	GM 1531	nepheline syenite		x	x		x	x						
Kûngnât	86182	gabbro	x	x		x	x			x	x			
	86186	gabbro	x	x		x	x			x	x			
	27685	syenogabbro	x	x		x	x			x	x			
	86194	syenite	x	x	x		x		x	x	x			
	86189	syenite	x	x	x		x		x	x	x			
	26119	syenite	x	x	x		x		x	x	x			
	81143	syenite	x	x	x		x		x	x	x			
	86200	syenite	x	x	x		x		x	x	x			
	81103	syenite	x	x	x		x		x	x	x			
	81108	syenite	x	x	x		x		x	x	x			
Motzfeld	JS 215	nepheline syenite		x	x		x	x			x			
	JS 105	nepheline syenite		x	x		x	x			x			
	JS 105	nepheline syenite		x	x		x	x			x			
	JS 181	larvikite	x	x	x	x	x	x		x	x			
Isortoq	GM 1682	anorthosite xenolith		x	x	x			x		x			
	GM 1803	gabbro	x	x		x	x			x	x			
	GM 1762	gabbro	x	x		x	x			x	x			
	GM 1761	gabbro	x	x		x	x			x	x			
	GM 1760	gabbro	x	x		x	x			x	x			
	GM 1712	syenogabbro		x		x	x			x	x			
	GM 1776	syenite		x	x		x			x	x			
	GM 1778	syenite		x	x		x			x	x			
	GM 1684	larvikite	x	x	x	x	x		x	x	x			
Tugtutôq (OGDC)	86120	gabbro	x	x		x				x	x			
	86122	gabbro	x	x		x				x	x			
	86126	syenogabbro	x	x	x	x	x			x	x			
	86100	syenite	x	x	x		x	x		x	x			
	86119	syenite	x	x	x		x	x		x	x			
	50241	pulaskite	x	x	x		x	x		x	x			
	86036	foyaite	x	x	x		x	x		x	x			
	86035	foyaite	x	x	x		x	x		x	x			
	85998	foyaite	x	x	x		x	x		x	x			
Tugtutôq (YGDC)	40452	gabbro	x	x		x				x	x			
	40464	gabbro	x	x		x				x	x			
	30636	gabbro	x	x		x				x	x			
	212103	gabbro	x	x		x				x	x			
	40551	syenogabbro	x	x	x	x	x			x	x			
	186221	syenogabbro	x	x	x	x	x			x	x			
	216621	syenogabbro	x	x	x	x	x			x	x			
	216622	syenite	x	x	x		x	x		x	x			
	186227	syenite	x	x	x		x	x		x	x			
	216627	syenite	x	x	x		x	x		x	x			
	40549	syenite	x	x	x		x		x	x	x			
Igdlutalik	101204	trachyte		x			x			x	x			
Puklen	GM 1634	syenite	x	x	x		x			x	x			
	GM 1590	syenite		x	x		x				x			
	GM 1625	syenite		x	x		x				x			
	GM 1586	syenite	x	x	x		x				x			
	GM 1615	syenite	x	x	x	x	x		x		x	x		
	GM 1616	syenite	x	x	x	x	x		x		x	x		
	GM 1605	granite		x	x	x	x		x		x			
	GM 1606	granite		x	x	x	x		x		x			
North Qoroq	DAR278	syenite		x	x		x	x			x			
Ilimaussaq	ILM 100	syenite	x	x	x		x			x	x			
	GM1858	syenite	x	x	x	x	x			x	x			
	GM1330	syenite	x	x	x		x	x		x	x			
	GM1332	syenite	x	x	x		x	x		x	x			
	GM1333	syenite	x	x	x		x	x		x	x			
	GM1333*	syenite	x	x	x		x	x		x	x			
	U-106	syenite	x	x	x		x			x	x			
	91937	syenite	x	x	x		x	x		x	x			
	50722	syenite	x	x	x		x	x		x	x			
	150772	syenite	x	x	x		x	x		x	x			

	P-1-5	pulaskite	x	x	x	x	x		x	x				
	91976	pulaskite	x	x	x	x	x		x	x				
	91943	foyaite	x	x	x	x	x		x	x				
	91980	foyaite	x	x	x	x	x		x	x				
	149532	agpaitic syenite	x	x	x	x	x		x	x	x	x	x	
	91922	agpaitic syenite		x	x	x	x				x	x	x	
	177244	agpaitic pegmatite		x	x	x		x					x	
	ID 3A	agpaitic vein		x	x	x		x			x	x	x	
	GM1852	phonolite	x	x	x	x	x			x	x	x	x	

Aen = aenigmatite ($Na_4[Fe^{2+}_{10}Ti_2]O_4[Si_{12}O_{36}]$); Eud = eudialyte ($Na_{15}Ca_6Fe_3Zr_3Si(Si_{25}O_{73})(O,OH,H_2O)_3(Cl,OH)_2$)